Journal of Computational Physics 242 (2013) 498–530

Contents lists available at SciVerse ScienceDirect

Journal of Computational Physics

journal homepage: www.elsevier.com/locate/jcp

# Variational integrators for electric circuits

Sina Ober-Blöbaum [a,*], Molei Tao [b], Mulin Cheng [d], Houman Owhadi [c,d], Jerrold E. Marsden [c,d,1]

[a] Computational Dynamics and Optimal Control, University of Paderborn, Germany
[b] Courant Institute of Mathematical Sciences, New York University, USA
[c] Control and Dynamical Systems, California Institute of Technology, USA
[d] Applied and Computational Mathematics, California Institute of Technology, USA

ARTICLE INFO

*Article history:*
Received 9 March 2011
Received in revised form 19 November 2012
Accepted 5 February 2013
Available online 20 February 2013

*Keywords:*
Structure-preserving integration
Variational integrators
Degenerate systems
Electric circuits
Noisy systems
Multiscale integration

ABSTRACT

In this contribution, we develop a variational integrator for the simulation of (stochastic and multiscale) electric circuits. When considering the dynamics of an electric circuit, one is faced with three special situations: 1. The system involves external (control) forcing through external (controlled) voltage sources and resistors. 2. The system is constrained via the Kirchhoff current (KCL) and voltage laws (KVL). 3. The Lagrangian is degenerate. Based on a geometric setting, an appropriate variational formulation is presented to model the circuit from which the equations of motion are derived. A time-discrete variational formulation provides an iteration scheme for the simulation of the electric circuit. Dependent on the discretization, the intrinsic degeneracy of the system can be canceled for the discrete variational scheme. In this way, a variational integrator is constructed that gains several advantages compared to standard integration tools for circuits; in particular, a comparison to BDF methods (which are usually the method of choice for the simulation of electric circuits) shows that even for simple LCR circuits, a better energy behavior and frequency spectrum preservation can be observed using the developed variational integrator.



## 1. Introduction

Variational integrators have mainly been developed and used for a wide variety of mechanical systems. However, real-life systems are generally not of purely mechanical character. In fact, more and more systems become multidisciplinary in the sense that not only mechanical parts but also electric and software subsystems are involved, which are called mechatronic systems. Since the integration of these systems with a unified simulation tool is desirable, the aim of this work is to extend the applicability of variational integrators to mechatronic systems. In particular, as the first step towards a unified simulation, we develop a variational integrator for the simulation of electric circuits.

*Overview.* Variational integrators [1] are based on a discrete variational formulation of the underlying system, for example based on a discrete version of Hamilton's principle for conservative mechanical systems. The resulting integrators, which are given by the discrete Euler–Lagrange equations, are symplectic and momentum-preserving and have an excellent long-time energy behavior. By choosing different variational formulations (e.g. Hamilton, Lagrange-d'Alembert, Hamilton-Pontryagin, etc.), variational integrators have been developed for classical conservative mechanical systems (for an overview see [2,3]), forced [4] and controlled [5] systems, constrained systems (holonomic [6,7] and nonholonomic systems [8]), nonsmooth systems [9], stochastic systems [10], and multiscale systems [11]. Most of these systems share the assumption that they are

* Corresponding author.
*E-mail address:* sinaob@math.upb.de (S. Ober-Blöbaum).
[1] Deceased.

0021-9991/$ - see front matter © 2013 Elsevier Inc. All rights reserved.
http://dx.doi.org/10.1016/j.jcp.2013.02.006

non-degenerate, that is the Legendre transformation of the corresponding Lagrangian is a diffeomorphism. By applying Hamilton's principle to a regular Lagrangian system, the resulting Euler–Lagrange equations are ordinary differential equations of second order and equivalent to Hamilton's equations.

The Lagrangian formulation for LC circuits is based on the electric and magnetic energies in the circuit and the interconnection constraints which are expressed in the Kirchhoff laws. There exists a large variety of different approaches for a Lagrangian or Hamiltonian formulation of electric circuits (see e.g. [12–16] and references therein). All of these authors treat the question of which choice of the Lagrangian coordinates and derivatives is the most appropriate one. Several settings have been proposed and analyzed, e.g. a variational formulation based on capacitor charges and currents, on inductor fluxes and voltages, and a combination of both settings, as well as formulations based on linear combinations of the charges and flux linkages. Typically, one wants to find a set of generalized coordinates such that the resulting Lagrangian is non-degenerate. However, within such a formulation, the variables are not easily interpretable in terms of original terms of a circuit.

A recently-considered alternative formulation is based on a redundant set of coordinates that results in a Lagrangian system for which the Lagrangian is degenerate. For a degenerate Lagrangian system, that is the Legendre transform is not invertible, the Euler–Lagrange equations involve additional hidden algebraic constraints. Then, the equations do not have a unique solution, and additional constraints are required for unique solvability of the system. For the circuit case, these are provided by the Kirchhoff Current Law (KCL). From a geometric point of view, the KCL provides a constraint distribution that induces a *Dirac structure* for the degenerate system. The associated system is called an *implicit Lagrangian system*. In [17,18], it was shown that nonholonomic mechanical systems and LC circuits as degenerate Lagrangian systems can be formulated in the context of induced Dirac structures and associated implicit Lagrangian systems. The variational structure of an implicit Lagrange system is given in the context of the Hamiltonian-Pontryagin-d'Alembert principle, as shown in [19]. The resulting Euler–Lagrange equations are called the *implicit Euler–Lagrange equations* [17,19,20], which are implicit differential–algebraic equations that consist of a system of first order differential equations and an additional algebraic equation that constrains the image of the Legendre transformation (called the *set of primary constraints*). Thus, the modeling of electric circuits involves both primary constraints as well as constraints coming from Kirchhoff's laws. In [21], an extension towards the interconnection of implicit Lagrange systems for electric circuits is demonstrated. For completeness, we have to mention that the corresponding notion of implicit Hamiltonian systems and implicit Hamiltonian equations was developed earlier by [22–24]. An intrinsic Hamiltonian formulation of dynamics of LC circuits as well as interconnections of Dirac structures have been developed, e.g. in [23,25], respectively.

There are only a few works dealing with the variational simulation of degenerate systems, e.g. in [26], variational integrators with application to point vertices as a special case of degenerate Lagrangian system are developed. Although there exists a variety of different variational formulations for electric circuits, variational integrators for their simulation have not been concretely investigated and applied thus far. In [27], a framework for the description of the discrete analogues of implicit Lagrangian and Hamiltonian systems is proposed. This framework is the foundation for the development of an integration scheme. However, no concrete simulation scenarios have yet been performed. Furthermore, the discrete formulation of the variational principle is slightly different from the approach presented in this work and thus, results in a different scheme.

*Contribution.* In this work, we present a unified variational framework for the modeling and simulation of electric circuits. The focus of our analysis is on the case of ideal linear circuit elements that consist of inductors, capacitors, resistors, and voltage sources. However, this is not a restriction of this approach, and the variational integrators can also be developed for nonlinear circuits, which is left for future work. A geometric formulation of the different possible state spaces for a circuit model is introduced. This geometric view point forms the basis for a variational formulation. Rather than dealing with Dirac structures, we work directly with the corresponding variational principle, where we follow the approach introduced in [19]. When considering the dynamics of an electric circuit, one is faced with three specific situations that lead to a special treatment within the variational formulation: 1. The system involves external (control) forcing through external (controlled) voltage sources. 2. The system is constrained via the Kirchhoff current (KCL) and voltage laws (KVL). 3. The Lagrangian is degenerate, which leads to primary constraints. For the treatment of forced systems, the Lagrange-d'Alembert principle is the principle of choice. By involving constraints, constrained variations are considered which results in a constrained principle. The degeneracy requires the use of the Pontryagin version; thus, the principle of choice is the constrained *Lagrange-d'Alembert-Pontryagin principle* [19]. Two variational formulations are considered: First, a constrained variational formulation is introduced for which the KCL constraints are explicitly given as algebraic constraints, whereas the KVL are given by the resulting Euler–Lagrange equations. Second, an equivalent reduced constrained variational principle is developed for which the KCL constraints are eliminated due to a representation of the Lagrangian on a reduced space. In this setting, the charges and flux linkages are the differential variables, whereas the currents play the role of algebraic variables. The number of inductors in the circuit and the circuit topology determine the degree of degeneracy of the system. For the reduced version, we show for which cases the degeneracy of the system is canceled via the KCL constraints. Based on the variational formulation, a variational integrator for electric circuits can be constructed. For the case of a degenerate system, the applicability of the variational integrator is dependent on the choice of discretization. Based on the type and order of the discretization, the degeneracy of the continuous system is canceled for the resulting discrete scheme. Three different integrators and their applicability to different electric circuits are investigated. The generality of a unified geometric (and discrete) variational formulation is advantageous for the analysis – for very complex circuits in particular.

By using the geometric approach, the main structure-preserving properties of the (discrete) Lagrangian system can be derived. In particular, as well known for symplectic integrators, good energy behavior can be observed for long time integra-

tion and for short simulation times with coarse time steps, whereas non-symplectic methods show significant distortions (e.g., in energy preservation). In presence of external forces (e.g., dissipation due to resistors), the correct rate of energy change is obtained. However, the main advantage of using variational integrators for electric circuits can be seen on the power spectra of the trajectories: the spectrum of high frequencies of the solutions is preserved without having to go for very long times. To the best of our knowledge, this has not been shown before. Furthermore, invariants (i.e., momentum maps due to symmetries of the Lagrangian system) can be derived and are preserved in the discrete solution. Going one step further, we extend the approach to a stochastic and multiscale setting. The generalization to a stochastic setting is motivated by the fact that real circuits are subject to, for instance, perturbations of the ambient electromagnetic fields, as well as dissipations due to self-resistance and self-radiation. The need for a multiscale extension is because modern circuits, for their functional purposes, are designed to exhibit dynamics over multiple time scales. Due to the variational framework, the resulting stochastic integrator well captures the statistics of the solution (see for instance [28]), and the resulting multiscale integrator is still variational [11].

*Outline.* In Section 2, we first review the basic notations for electric circuits and introduce a graph representation to describe the circuit topology. In addition, we introduce a geometric formulation that gives an interpretation of the different state spaces of a circuit model. Based on the geometric view point, the two (reduced and unreduced) variational formulations are derived in Section 3. The equivalence of both formulations as well as conditions for obtaining a non-degenerate reduced system are proven. In Section 4, the construction of different variational integrators for electric circuits is described, and conditions for their applicability are derived. The main structure-preserving properties of the Lagrangian system and the variational integrator are summarized in Section 5. In Section 6, the approach is extended for the treatment of noisy circuits. In Section 7, the efficiency of the developed variational integrators is demonstrated by means of numerical examples. A comparison with standard circuit modeling and circuit integrators is given. In particular, the applicability of the multiscale method FLAVOR [11] is demonstrated for a circuit with different time scales.

## 2. Electric circuits

### 2.1. Basic notations

For an electric circuit, we introduce the following notations (following [29]): A *node* is a point in the circuit where two or more elements meet. A *path* is a trace of adjoining circuit elements with no elements included more than once. That means it is a union of adjoining basic elements for which each element is included at most ones. A *branch* is a path that connects two nodes. A *loop* is a path that begins and ends at the same node. A *mesh* (also called *fundamental loop*) is a loop that does not enclose any other loops. A *planar circuit* is a circuit that can be drawn on a plane without crossing branches.

Let $q(t), v(t), u(t) \in \mathbb{R}^n$ be the time-dependent charges, the currents, and the voltages of the circuit elements with $t \in [0, T]$, where $q_J(t), v_J(t), u_J(t) \in \mathbb{R}^{n_J} (J \in \{L, C, R, V\})$ are the corresponding quantities through the $n_L$ inductors, the $n_C$ capacitors, the $n_R$ resistors, and the $n_V$ voltage sources. In addition, we give each of those devices an assumed current flow direction. In Table 1, the characteristic equations for basic elements are listed. For the analysis in this work, we focus on ideal linear circuit elements, that is we consider the following constitutive laws for each element ($n_J = 1, J \in \{L, C, R\}$):

$$u_L(t) = L\dot{v}_L(t), \quad v_C(t) = C\dot{u}_C(t), \quad u_R(t) = Rv_R(t),$$

with inductance $L$, capacitance $C$, and resistance $R = G^{-1}$ with conductance $G$ and where in general we have $\dot{q}(t) = v(t)$. The flux linkage for each element is denoted by $p(t) \in \mathbb{R}^n$ and for an inductor, it is defined as the time integral of the voltage across the inductor. Note that in the case of an inductor (resp. a capacitor), the associated charge $q_L$ (resp. flux linkage $p_C$) is an artificial variable. Similarly, for the resistors and the voltage sources, the associated charges $q_R, q_V$ and flux linkages $p_R, p_V$ are artificial variables.

Ideal inductors and capacitors are purely reactive, that is they dissipate no energy. Thus, the magnetic energy stored in one inductor with inductance $L$ is

$$E_{\text{mag}} = \frac{1}{2} L v_L^2.$$

**Table 1**
Characteristic equations for basic circuit elements.

| Device | Linear | Nonlinear |
|---|---|---|
| Resistor | $v_R = Gu_R$ | $v_R = g(u_R, t)$ |
| Capacitor | $v_C = C\frac{d}{dt}u_C$ | $v_C = \frac{d}{dt}q_C(u_C, t)$ |
| Inductor | $u_L = L\frac{d}{dt}v_L$ | $u_L = \frac{d}{dt}p_L(v_L, t)$ |
| Device | Independent | Controlled |
| Voltage source | $u_V = v(t)$ | $u_V = v(u_{ctrl}, v_{ctrl}, t)$ |
| Current source | $v_I = i(t)$ | $v_I = v(u_{ctrl}, v_{ctrl}, t)$ |

The amount of energy storage in one capacitor with capacitance $C$ is

$$E_{\mathrm{el}} = \int_{q=0}^{q_C} u_C \, dq = \int_{q=0}^{q_C} \frac{q}{C} \, dq = \frac{1}{2}\frac{1}{C} q_C^2.$$

### 2.2. Graph representation

Consider now a circuit as a connected, directed graph with $n$ edges and $m+1$ nodes. On the $i$th edge, there are: a capacitor with capacitance $C_i$, an inductor with inductance $L_i$, a voltage source $\epsilon_i$, and a resistor with resistance $R_i$, one or several of which can be zeros (cf. Fig. 1). Thus, branches in the circuit correspond to edges in the graph. In the special case that each edge in the graph represents only one circuit element, the number of edges in the graph equals the number of circuit elements, and the number of nodes of the circuit and the graph are the same. For simplicity, we use the notions from circuit theory, that is we talk about branches and meshes in the graph.

For the analysis with circuits, one is faced with the following two basic laws:

1. The Kirchhoff Current Law (KCL) states that the sum of currents leading to and leaving from any node is equal to zero.
2. The Kirchhoff Voltage Law (KVL) states that the sum of voltages along each mesh (or fundamental loop) of the network is equal to zero.

Let $K \in \mathbb{R}^{n,m}$ be the *Kirchhoff Constraint matrix* of a given circuit that is represented via a graph defined by

$$K_{ij} = \begin{cases} -1 & \text{branch } i \text{ connected inward to node } j \\ +1 & \text{branch } i \text{ connected outward to node } j \\ 0 & \text{otherwise.} \end{cases} \tag{1}$$

In the special case where the two ends of an edge are connected to the same node, we set $K_{ij} = 0$. Since the ground node is excluded, the Kirchhoff Constraint matrix has only $m$ rather than $m+1$ columns. Allowing only one circuit element for one branch, either inductor, capacitor, resistor, or voltage source, $K$ can be expressed as

$$K = \begin{pmatrix} K_L \\ K_C \\ K_R \\ K_V \end{pmatrix},$$

where $K_J \in \mathbb{R}^{n_J,m} (J \in \{L, C, R, V\})$ is the Constraint Matrix for the set of $n_L$ inductors, $n_C$ capacitors, $n_R$ resistors, and $n_V$ voltage sources, respectively with $n_L + n_C + n_R + n_V = n$. The Kirchhoff Constraint Matrix provides the Kirchhoff current constraints as $K^T v = 0$. For connected, planar graphs, the number of meshes $l$ is determined via $l = n - m$, where $n$ is the number of branches and $m+1$ the number of nodes. This is a direct consequence from Euler's formula [30]. We can thus define the *Fundamental Loop matrix* $K_2 \in \mathbb{R}^{n,n-m}$ by

$$K_{2,ij} = \begin{cases} -1 & \text{branch } i \text{ is a backward branch in mesh } j \\ +1 & \text{branch } i \text{ is a forward branch in mesh } j \\ 0 & \text{branch } i \text{ does not belong to mesh } j, \end{cases} \tag{2}$$

where again $K_2$ can be expressed as

$$K_2 = \begin{pmatrix} K_{2,L} \\ K_{2,C} \\ K_{2,R} \\ K_{2,V} \end{pmatrix},$$

with $K_{2,J} \in \mathbb{R}^{n_J,n-m} (J \in \{L, C, R, V\})$ being the Loop Matrix for the set of $n_L$ inductors, $n_C$ capacitors, $n_R$ resistors, and $n_V$ voltage sources, respectively. The Fundamental Loop Matrix provides the Kirchhoff voltage constraints as $K_2^T u = 0$. An alternative expression of the Kirchhoff voltage constraints is given by $K\hat{u} = u$, where $\hat{u}$ are the node voltages of the circuit. By $u \in ker(K_2^T)$ and $u \in im(K)$ it follows directly that $ker(K_2^T) = im(K)$ and thus $im(K_2) \perp im(K)$.

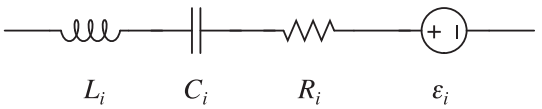


**Fig. 1.** A typical branch of a circuit. On this edge, there are: an inductor $L_i$, a capacitor $C_i$, a resistor $R_i$, and a voltage source $\epsilon_i$, one or several of which can be zeros.

### 2.3. Geometric setting

By using a geometric approach for the analysis of circuits, we define the configuration manifold to be the *charge space* $Q \subseteq \mathbb{R}^n$ of circuit branches with points on the manifold denoted by $q \in Q$. For a particular charge configuration $q$, the tangent bundle $TQ$ is the *current space* with currents $v \in T_qQ \subseteq \mathbb{R}^n$ passing through the branches. The corresponding cotangent bundle $T^*Q$ is the *flux linkage space* with the flux linkages $p \in T_q^*Q \subseteq \mathbb{R}^n$. Note that due to the analogy with the quantities, configuration, velocity, and momentum in mechanical systems, we stick with the notation $(q, v, p)$ for charge, current, and flux linkage. The branch voltages $u$ are the analogy with forces for the mechanical system and are thus assumed to be covectors in the cotangent space $T_q^*Q$.

Let $\Delta_Q \subset TQ$ be a constraint distribution, which is locally given by

$$\Delta_Q(q) = \{v \in T_qQ \,|\, \langle w^a, v\rangle = 0, a = 1, \dots, m\} \subset T_qQ, \tag{3}$$

with the natural pairing $\langle\cdot,\cdot\rangle : T_q^*Q \times T_qQ \to \mathbb{R}$ of cotangent and tangent vectors. $w^a$ are $m$ independent one-forms that form the basis for the annihilator $\Delta_Q^0(q) \subset T^*Q$, which is locally given by

$$\Delta_Q^0(q) = \{w \in T_q^*Q \,|\, \langle w, v\rangle = 0 \,\forall v \in \Delta_Q(q)\} \subset T_q^*Q. \tag{4}$$

$\Delta_Q(q)$ and $\Delta_Q^0(q)$ are spaces of dimension $n-m$ and $m$, respectively, and embedded in $T_qQ$ and $T_q^*Q$, respectively, with local representatives being in $\mathbb{R}^n$.

By using the matrix $K^T$ as local coordinate representation for the one-forms $w^a$, the distribution (3) forms the *constraint KCL space* given by the submanifold

$$\Delta_Q(q) = \{v \in T_qQ \,|\, K^T v = 0\} \subset T_qQ,$$

which is spanned by $ker(K^T)$. Note that since Since $K$ is constant, $\Delta_Q(q)$ is integrable and thus holonomic. Its annihilator $\Delta_Q^0(q)$ can thus be locally expressed by the image $im(K)$ of $K$. By choosing this coordinate representation and with $ker(K_2^T) = im(K)$, the annihilator (4) decribes the *constraint KVL space* by

$$\Delta_Q^0(q) = \{u \in T_q^*Q \,|\, K_2^T u = 0\} \subset T_q^*Q.$$

Note that the choices of $K$ and $K_2$ are in general not unique. The only design criterion for $K_2$ is the condition $im(K) \perp im(K_2)$. Alternative to (2), a matrix $K_2$ can be constructed using a QR-decomposition of $K$. Thus, this approach is not restricted to cases, where the mesh topology is obvious as for planar graphs. However, in the following we work with the Fundamental Loop matrix as candidate for the matrix $K_2$ due to the physical interpretation.

From a geometric point of view, we can distinguish between three different spaces: Let $\mathfrak{B}$ denote the space of branches, $\mathfrak{M}$ the space of meshes, and $\mathfrak{N}$ the space of nodes, where we exclude the one node defined as ground. $(q, v, p, u)$ denote the branch charges, currents, flux linkages, and voltages, and $(\tilde{q}, \tilde{v}, \tilde{p}, \tilde{u})$ and $(\hat{q}, \hat{v}, \hat{p}, \hat{u})$ the corresponding quantities in mesh and node space, respectively. From KCL and KVL, we know that the node currents (and charges) as well as the mesh voltages are zero. For $\mathfrak{M}$ and $\mathfrak{N}$, we define the corresponding configuration, tangent and cotangent spaces $M \subseteq \mathbb{R}^{n-m}, T_{\tilde{q}}M \subseteq \mathbb{R}^{n-m}, T_{\tilde{q}}^*M \subseteq \mathbb{R}^{n-m}$, and $N \subseteq \mathbb{R}^m, T_{\hat{q}}N \subseteq \mathbb{R}^m, T_{\hat{q}}^*N \subseteq \mathbb{R}^m$. Then, branch, loop, and node space are defined to be the Pontryagin bundle which is the direct sum of tangent and cotangent space, that is $\mathfrak{B} = \Delta_Q \oplus \Delta_Q^0, \mathfrak{M} = TM \oplus T^*M$, and $\mathfrak{N} = TN \oplus T^*N$.

The following diagram gives the relation between the defined spaces in terms of the Kirchhoff Constraint matrix $K$ and the Fundamental Loop matrix $K_2$

$$\begin{array}{ccccc} T_{\hat{q}}^*N & \xrightarrow{K} & \Delta_Q^0(q) & \xrightarrow{K_2^T} & \{0\} \subset T_{\tilde{q}}^*M \\ \mathfrak{N} & & \mathfrak{B} & & \mathfrak{M} \\ \text{nodes} & & \text{branches} & & \text{meshes} \\ \{0\} \subset T_{\hat{q}}N & \xleftarrow{K^T} & \Delta_Q(q) & \xleftarrow{K_2} & T_{\tilde{q}}M \end{array} \tag{5}$$

with the linear maps $K : T_{\hat{q}}^*N \to \Delta_Q^0(q)$ and $K_2 : T_{\tilde{q}}M \to \Delta_Q(q)$, and their adjoints $K^T : \left(\Delta_Q^0(q)\right)^* \to T_{\hat{q}}N$ and $K_2^T : (\Delta_Q(q))^* \to T_{\tilde{q}}^*M$. Note that $K^T$ restricted to $\Delta_Q(q) \subset \left(\Delta_Q^0(q)\right)^*$ maps to $\{0\} \subset T_{\hat{q}}N$, and $K_2^T$ restricted to $\Delta_Q^0(q) \subset (\Delta_Q(q))^*$ maps to $\{0\} \subset T_{\tilde{q}}^*M$. This corresponds to the fact that, as stated above, the branch currents that are consistent with the KCL are determined by $ker(K^T)$, where the branch voltages that are consistent with the KVL are given by $ker(K_2^T)$. On the other hand, from diagram (5), we can directly follow that the set of branch currents that satisfy the KCL can alternatively be expressed as $v = K_2\tilde{v}$, whereas the set of branch voltages that satisfy the KVL are in the image of $K$ as $u = K\hat{u}$. These are the standard relations between branch currents $v(t)$ and mesh currents $\tilde{v}(t)$, and branch voltages $u(t)$ and node voltages $\hat{u}(t)$, respectively, given by KCL and KVL. Note that diagram (5) represents the general relations between the tangent spaces $T_qQ, T_{\hat{q}}N$, and $T_{\tilde{q}}M$, and the corresponding cotangent spaces. The matrices $K$ and $K_2$ are local coordinate choices for the projections to the different spaces. These are not unique. However, by using different coordinates representations, the submanifolds $T_{\hat{q}}N, T_{\hat{q}}^*N, T_{\tilde{q}}M$, and $T_{\tilde{q}}^*M$ lose their physical meaning.

Following the lines of [19], the tangent space at $q$ can be split such that $T_qQ = \mathcal{H}_q \oplus \mathcal{V}_q$, where $\mathcal{H}_q = \Delta_q(q)$ is the *horizontal space* and $\mathcal{V}_q$ the *vertical space* at $q$. The matrix $K^T$ is a local matrix representation of the *Ehresmann connection* $A_q : T_qQ \to \mathcal{V}_q$.

**Remark 1.** A branch can consist of more than one circuit element in a row. In this case, the branch voltage is assumed to be the sum of the voltages of all elements in this branch.

## 3. Variational formulation for electric circuits

In the following, we derive the equations of motion for the circuit system by making use of variational principles that are known in mechanics. We present two different variational formulations that distinguish in the way the constraints (KCL and KVL) are involved.

### 3.1. Constrained variational formulation

We can define a Lagrangian $\mathcal{L} : TQ \to \mathbb{R}$ of the circuit system that consists of the difference between magnetic and electric energy as

$$\mathcal{L}(q, v) = \frac{1}{2} v^T L v - \frac{1}{2} q^T C q, \tag{6}$$

with $L = \mathrm{diag}(L_1, \ldots, L_n)$ and $C = \mathrm{diag}\left(\frac{1}{C_1}, \ldots, \frac{1}{C_n}\right)$. In the case where no inductor (resp. no capacitor) is on branch $i$, the corresponding entry $L_i$ (resp. $\frac{1}{C_i}$) in the matrix $L$ (resp. $C$) is zero. In the presence of mutual inductors rather than self inductors, the matrix $L$ is not diagonal anymore but always positive semi-definite. Unless explicitly mentioned, the following theory and construction are also valid for mutual inductors. The Legendre transform $\mathbb{F}\mathcal{L} : TQ \to T^*Q$ is defined by

$$\mathbb{F}\mathcal{L}(q, v) = (q, \partial\mathcal{L}/\partial v) = (q, Lv). \tag{7}$$

Note that the Lagrangian can be degenerate if the Legendre transform is not invertible. The *constraint flux linkage subspace*[2] is defined by the Legendre transform as

$$P = \mathbb{F}\mathcal{L}(\Delta_Q) \subset T^*Q,$$

where $\Delta_Q \subset TQ$ is the distribution. The Lagrangian force of the system consists of a damping force that results from the resistors and an external force being the voltage sources

$$f_L(q, v, t) = -\mathrm{diag}(R)\, v + \mathrm{diag}(\mathcal{E})u, \tag{8}$$

with $R = (R_1, \ldots, R_n)^T$ and $\mathcal{E} = (\epsilon_1, \ldots, \epsilon_n)^T$. If no resistor is on branch $i$, the corresponding entry $R_i$ in the vector $R$ is zero. For the entries of the vector $\mathcal{E}$, we have $\epsilon_i = 0$ if no voltage source is on branch $i$ and $\epsilon_i = 1$ otherwise. Here, we assume that the time evolution of the voltage sources is given as time dependent function $u_s(t)$. Thus, in the following, we replace $\mathrm{diag}(\mathcal{E})u$ by $u_s(t)$ for a given function $u_s : [0, T] \to \mathbb{R}^n$.

To derive the equations of motion for the circuit system, we make use of the Lagrange-d'Alembert-Pontryagin principle, that is we are searching for curves $q(t)$, $v(t)$, and $p(t)$ that satisfy $d\mathfrak{S}(q, v, p)(\delta q, \delta v, \delta p) = 0$. This gives

$$\delta \int_0^T \mathcal{L}(q(t), v(t)) + \langle p(t), \dot{q}(t) - v(t)\rangle\, dt + \int_0^T f_L(q(t), v(t), t) \cdot \delta q(t)\, dt = 0, \tag{9}$$

with fixed initial and final variations $\delta q(0) = \delta q(T) = 0$ and constrained variations $\delta q \in \Delta_Q(q)$.

Taking variations gives us

$$\int_0^T \left[\left\langle \frac{\partial\mathcal{L}}{\partial q} + f_L, \delta q \right\rangle - \langle \dot{p}, \delta q\rangle + \langle \delta p, \dot{q} - v\rangle + \left\langle \left(\frac{\partial\mathcal{L}}{\partial v}\right) - p, \delta v \right\rangle\right] dt = 0 \tag{10}$$

for arbitrary variations $\delta v$ and $\delta p, K^T v = 0$ and constrained variations $\delta q \in \Delta_Q(q)$. This leads to the constrained Euler–Lagrange equations

$$\frac{\partial\mathcal{L}}{\partial q} - \dot{p} + f_L \in \Delta_Q^0(q), \tag{11a}$$

$$\dot{q} = v, \tag{11b}$$

$$\frac{\partial\mathcal{L}}{\partial v} - p = 0, \tag{11c}$$

[2] Also denoted by the set of primary constraints.

$$K^T v = 0. \tag{11d}$$

For the Lagrangian (6) and the forces (8), the constrained Euler–Lagrange equations are

$$\dot{p} = -Cq - \operatorname{diag}(R)v + u_s + K\lambda, \tag{12a}$$

$$\dot{q} = v, \tag{12b}$$

$$p = Lv, \tag{12c}$$

$$K^T v = 0, \tag{12d}$$

where $\lambda$ represent the node voltages $\hat{u} \in T^*N$. Thus, the first line corresponds to the KVL equations of the form $K\hat{u} = u$, and the last line are the KCL equations. System (12) is a differential–algebraic system with differential variables $q$ and $p$ and algebraic variables $v$ and $\lambda$. The involvement of the function $u_s(t)$ makes the system a non-autonomous system. Eq. (12c) (also denoted by primary constraints) reflects the degeneracy of the Lagrangian system: since $\mathbb{F}\mathcal{L}$ is not invertible (i.e., $L$ is singular), we can not eliminate the algebraic variable $v$ to obtain a purely Hamiltonian formulation. However, in the next step, we eliminate the algebraic variable $\lambda$ by the use of a reduced constrained variational principle.

### 3.2. Reduced constrained variational formulation

With the following reduced principle, we derive a slightly different form of the resulting differential–algebraic system. This reduced formulation is advantageous from different perspectives: First, the reduced formulation is less redundant such that the Lagrange multipliers are eliminated and the state space dimension is reduced. Second, for specific circuits, the degeneracy of the Lagrangian is canceled. Third, the reduced state space still has a physical and geometric interpretation: The reduced Lagrangian is defined on the mesh space $TM \subseteq \mathbb{R}^{2(n-m)}$ rather than on the branch space $TQ \subseteq \mathbb{R}^{2n}$.

For the reduction, instead of treating the KCL as extra constraint in the form $K^T v = 0$, we directly involve the KCL form $K_2\tilde{v} = v$ with $\tilde{v} \in T_qM \subseteq \mathbb{R}^{n-m}$ for the definition of the new Lagrangian system. Since $K$ is constant, the constraints are integrable, that is the configurations $q$ are constrained to be in the submanifold

$$\mathcal{C} = \{q \in Q \,|\, K^T q = 0\}$$

for consistent initial values $q_0 \in \mathcal{C}$. This simply means that topological relationships that apply for currents is also satisfied for charges up to a constant vector. Then, we have $T_q\mathcal{C} = \Delta_Q(q)$ and the branch charges $q$ can be expressed by the mesh charges $\tilde{q} \in M \subseteq \mathbb{R}^{n-m}$ as $q = K_2\tilde{q}$. We define the reduced Lagrangian $\mathcal{L}^M : TM \to \mathbb{R}$ via pullback as $\mathcal{L}^M := K_2^*\mathcal{L} : TM \to \mathbb{R}$ with

$$\mathcal{L}^M(\tilde{q}, \tilde{v}) = \mathcal{L}(K_2\tilde{q}, K_2\tilde{v}) = \frac{1}{2}\tilde{v}^T K_2^T L K_2 \tilde{v} - \frac{1}{2}\tilde{q}^T K_2^T C K_2 \tilde{q} \tag{13}$$

with the Legendre transform $\mathbb{F}\mathcal{L}^M : TM \to T^*M$

$$\mathbb{F}\mathcal{L}^M(\tilde{q}, \tilde{v}) = (\tilde{q}, \partial\mathcal{L}^M/\partial\tilde{v}) = (\tilde{q}, K_2^T L K_2 \tilde{v}).$$

Dependent on the inductor matrix $L$ and the graph topology, the matrix $K_2^T L K_2$ can still be singular, that is the Lagrangian system can still be degenerate. The cotangent bundle $T^*M$ is given by

$$T^*M = \{(\tilde{q}, \tilde{p}) \in \mathbb{R}^{n-m,n-m} \,|\, (\tilde{q}, \tilde{p}) = \mathbb{F}\mathcal{L}^M(\tilde{q}, \tilde{v}) \text{ with } (\tilde{q}, \tilde{v}) \in TM\} = \{(\tilde{q}, \tilde{p}) \in \mathbb{R}^{n-m,n-m} \,|\, (\tilde{q}, \tilde{p}) = (\tilde{q}, K_2^T p) \text{ with } p \in P\}.$$

Thus, the reduced force $f_L^M$ in $T^*M$ is defined as

$$f_L^M(\tilde{q}, \tilde{v}, t) = K_2^T f_L(K_2\tilde{q}, K_2\tilde{v}, t) = -K_2^T \operatorname{diag}(R) K_2 \tilde{v} + K_2^T u_s(t). \tag{14}$$

With $\tilde{p} \in T_{\tilde{q}}^*M \subset \mathbb{R}^{n-m}$ given as $\tilde{p} = K_2^T p$ we obtain the following reduced Lagrange-d'Alembert-Pontryagin principle

$$\delta \int_0^T \mathcal{L}^M(\tilde{q}(t), \tilde{v}(t)) + \left\langle \tilde{p}(t), \dot{\tilde{q}}(t) - \tilde{v}(t) \right\rangle dt + \int_0^T f_L^M(\tilde{q}(t), \tilde{v}(t), t) \cdot \delta\tilde{q}(t)\, dt = 0, \tag{15}$$

with fixed initial and final variations $\delta\tilde{q}(0) = \delta\tilde{q}(T) = 0$. Taking variations gives us

$$\int_0^T \left[ \left\langle \frac{\partial\mathcal{L}^M}{\partial\tilde{q}} + f_L^M, \delta\tilde{q} \right\rangle - \langle \dot{\tilde{p}}, \delta\tilde{q} \rangle + \left\langle \delta\tilde{p}, \dot{\tilde{q}} - \tilde{v} \right\rangle + \left\langle \left( \frac{\partial\mathcal{L}^M}{\partial\tilde{v}} \right) - \tilde{p}, \delta\tilde{v} \right\rangle \right] dt = 0 \tag{16}$$

for arbitrary variations $\delta\tilde{v}, \delta\tilde{p}$, and $\delta\tilde{q}$. This results in the reduced Euler–Lagrange equations

$$\frac{\partial \mathcal{L}^M}{\partial \tilde{q}} - \dot{\tilde{p}} + f_L^M = 0, \tag{17a}$$

$$\dot{\tilde{q}} = \tilde{v}, \tag{17b}$$

$$\frac{\partial \mathcal{L}^M}{\partial \tilde{v}} - \tilde{p} = 0. \tag{17c}$$

For the Lagrangian (13) and the forces (14), the reduced Euler–Lagrange equations are

$$\dot{\tilde{p}} = K_2^T(-CK_2\tilde{q} - \mathrm{diag}(R)K_2\tilde{v} + u_s), \tag{18a}$$

$$\dot{\tilde{q}} = \tilde{v}, \tag{18b}$$

$$\tilde{p} = K_2^T L K_2 \tilde{v}. \tag{18c}$$

Here, the first equation is now the KVL in the form $K_2^T u = 0$, in which the KCL in the form $K_2\tilde{v} = v$ is also involved. System (18) is a differential–algebraic system with differential variables $\tilde{q}$ and $\tilde{p}$ and algebraic variables $\tilde{v}$. The algebraic Eq. (18c) is the Legendre transformation of the system. If this is invertible (i.e., the matrix $K_2^T L K_2$ is regular), the algebraic variable $v$ can be eliminated. In this case, the Euler–Lagrange Eq. (18) represent a non-degenerate Lagrangian system.

**Remark 2.** In classical geometric mechanics, the terminology "reduction" is mainly utilized for symmetry reduction in mechanics. However, in this contribution, we refer to reduction under constraints and not under symmetries, that is the dimension $n$ of the tangent space $TC$ is decreased (reduced) to $n - m$ by choosing a new parametrization of variables.

In the following proposition, we show for which cases the reduced Lagrangian system is non-degenerate for LC circuits, that is for which cases the KVL cancels the degeneracy. The statements for RCL and RCLV circuits can be derived in an analogous way (see Remark 3(b)).

**Proposition 1.** *For LC circuits (including only self inductors), the system is non-degenerate if the number of capacitors equals the number of independent constraints that involve the currents through the capacitives branches.*

**Proof.** We have to show that $ker(K_2^T L K_2) = \{0\}$. Let $n_C$ be the number of capacitors and $m$ the number of Kirchhoff Constraints such that $K_C^T \in \mathbb{R}^{m,n_C}$. Let $l_C \leqslant m$ be the number of independent constraints involving the currents through the capacitives branches. With $n_C = l_C \leqslant m$ we have $rank(K_C^T) = n_C$, thus $ker(K_C^T) = \{0\}$. On the other hand, we have

$$ker(L) = \{v \in T_qQ \,|\, v_L = 0\}$$

and

$$\mathcal{R}(K_2) = ker(K^T) = \{v \in T_qQ \,|\, K^T v = 0\} = \left\{ v \in T_qQ \,|\, (K_L^T K_C^T)\begin{pmatrix} v_L \\ v_C \end{pmatrix} = 0 \right\},$$

With $ker(K_C^T) = \{0\}$ this results in

$$\mathcal{R}(K_2) \cap ker(L) = \{v \in T_qQ \,|\, K_C^T v_C = 0\} = \{0\} \tag{19}$$

and thus $ker(LK_2) = \{0\}$. Since $L$ is a diagonal matrix, we can split $K_2^T L K_2$ into $K_2^T \sqrt{L}^T \sqrt{L} K_2$, where $\sqrt{L}$ corresponds to the diagonal matrix with diagonal elements $\sqrt{L_i}, L_i > 0$, $i = 1, \ldots, n$. Since $K_2$ has full column rank, we know with (19) that $\sqrt{L}K_2$ also has full column rank. It follows for $y \in \mathbb{R}^{n-m}$ and $y \in ker(K_2^T L K_2)$ that

$$K_2^T L K_2 y = 0 \Rightarrow y^T K_2^T L K_2 y = 0 \Longleftrightarrow y^T K_2^T \sqrt{L}^T \sqrt{L} K_2 y = 0 \Longleftrightarrow \|\sqrt{L}K_2 y\|_2 = 0$$

and thus $y = 0$ since $ker(\sqrt{L}K_2) = \{0\}$. We therefore have $ker(K_2^T L K_2) = ker(\sqrt{L}K_2) = \{0\}$ and the matrix $K_2^T L K_2$ is invertible. □

**Remark 3.**

(a) Intuitively spoken, the degeneracy of the original Lagrangian is due to the lack of magnetic energy terms for the capacitors. With each independent constraint on the capacitor currents, one degree of freedom of the system can be removed. Hence, as many capacitors constraints are required to remove the capacitor current (cf. [14]).
(b) In addition, for a RLC (resp. RCLV) non-degenerate circuit, the number of resistors (resp. and voltage sources) has to equal the number of independent constraints that involve the currents through the resistor (resp. and voltage source) branches.

**Theorem 1** (*Equivalence*). *The system (11) and the reduced system (17) are equivalent in the following sense:*

*(i) Let $(\tilde{q},\tilde{p},\tilde{v})$ be a solution of the reduced system (17) and let $q = K_2\tilde{q}$, $v = K_2\tilde{v}$ and $(q,p) = \mathbb{F}\mathcal{L}(q,v)$. Then $(q,v,p)$ is a solution to system (11) and we have $\tilde{p} = K_2^T p$.*

*(ii) Let $(q,v,p)$ be a solution to system (11) and $\tilde{q} = K_2^+ q$, $\tilde{v} = K_2^+ v$ and let $\tilde{p} = K_2^T p$ with the well-defined pseudo-inverse $K_2^+$ of $K_2$ (with $K_2^+ K_2 = I$). Then $(\tilde{q},\tilde{p},\tilde{v})$ is a solution of the reduced system (17).*

**Proof.**

(i) Assume that $(\tilde{q},\tilde{p},\tilde{v})$ is a solution of (17). From the assumption $p = \mathbb{F}L(q,v)$ it follows that $p - \frac{\partial}{\partial v}\mathcal{L}(q,v) = 0$. With $\mathcal{L}^M = K_2^*\mathcal{L}$ we have

$$\frac{\partial \mathcal{L}^M}{\partial \tilde{q}}(\tilde{q},\tilde{v}) = \frac{\partial \mathcal{L}}{\partial \tilde{q}}(K_2\tilde{q},K_2\tilde{v}) = \left(\frac{\partial q}{\partial \tilde{q}}\right)^T \frac{\partial \mathcal{L}}{\partial q}(K_2\tilde{q},K_2\tilde{v}) = K_2^T \frac{\partial \mathcal{L}}{\partial q}(q,v).$$

Similarly, we have $\frac{\partial \mathcal{L}^M}{\partial \tilde{v}}(\tilde{q},\tilde{v}) = K_2^T \frac{\partial \mathcal{L}}{\partial v}(q,v)$ and thus, it follows that

$$\tilde{p} = \frac{\partial \mathcal{L}^M}{\partial \tilde{v}}(\tilde{q},\tilde{v}) = K_2^T \frac{\partial \mathcal{L}}{\partial v}(q,v) = K_2^T p.$$

Together with (14), this gives

$$K_2^T \dot{p} = \dot{\tilde{p}} = \frac{\partial \mathcal{L}^M}{\partial \tilde{q}} + f_L^M = K_2^T\left(\frac{\partial \mathcal{L}}{\partial q} + f_L\right) \Rightarrow K_2^T\left(\frac{\partial \mathcal{L}}{\partial q} - \dot{p} + f_L\right) = 0 \Rightarrow \frac{\partial \mathcal{L}}{\partial q} - \dot{p} + f_L \in ker(K_2^T).$$

With $ker(K_2^T) = im(K)$, it follows that

$$\frac{\partial \mathcal{L}}{\partial q} - \dot{p} + f_L \in im(K) = \Delta_Q^0(q)$$

as can be seen from diagram (5). Furthermore, we have

$$\dot{q} = K_2\dot{\tilde{q}} = K_2\tilde{v} = v$$

and since we have $v = K_2\tilde{v}$, from diagram (5) it follows that $K^T v = 0$. Both expressions are equivalent formulations of the KCL.

(ii) Now assume that $(q,p,v)$ is a solution of (11). With $ker(K_2^T) = im(K)$ and (14), it follows immediately that

$$\dot{\tilde{p}} = K_2^T \dot{p} = K_2^T\left(\frac{\partial \mathcal{L}}{\partial q} + f_L\right) = \frac{\partial \mathcal{L}^M}{\partial \tilde{q}} + f_L^M.$$

Furthermore, from $\dot{q} = v$ we get $K_2^+\dot{q} = K_2^+ v$ which gives $\dot{\tilde{q}} = \tilde{v}$. Finally, we have $\tilde{p} = K_2^T p = K_2^T \frac{\partial \mathcal{L}}{\partial v} = \frac{\partial \mathcal{L}^M}{\partial \tilde{v}}$ □.

**Remark 4.** We require the assumption $(q,p) = \mathbb{F}L(q,v)$ (the fulfillment of the Legendre transformation) in Theorem 1(i) for the fulfillment of the relation (11c). A unique derivation of $p$ directly from $\tilde{p}$ is in general not possible from $\tilde{p} = K_2^T p$ as it is for $q$ and $v$: Although there is a canonical projection $K_2^T : T^*Q \to T^*M$, there is no corresponding canonical projection of $T^*M$ into $T^*Q$ (see also [1]). By assuming that $\tilde{p} = K_2^T p$ instead of $(q,p) = \mathbb{F}L(q,v)$ in (i), we only get the relation $K_2^T(p - \partial\mathcal{L}/\partial v) = 0$, and (11c) may not be satisfied.

**Remark 5.** Statement (i) of Theorem 1 can be interpreted as reconstruction from a given solution on the constrained manifold $TM \oplus T^*M$ while statement (ii) defines a map $\Delta_Q \oplus (\Delta_Q)^* \to TM \oplus T^*M$ given by $(K_2^+, K_2^+, K_2^T)$.

## 4. Discrete variational principle for electric circuits

In this section, we derive a discrete variational principle that leads to a variational integrator for the circuit system. Since the solution of the reduced system (17) can be easily transformed to a solution of the full system (11) (Theorem 1), we restrict the discrete derivation to the reduced case. For the case of a degenerate reduced system, the choice of discretization is important to obtain a variational integrator that manages to bypass the difficulty of intrinsic degeneracy, and thus, is applicable for a simulation. In this section, three different discretizations are introduced that result in three different discrete variational schemes for which the solvability conditions are derived.

For the discrete variational derivation, we introduce a discrete time grid $\Delta t = \{t_k = kh \,|\, k = 0,\dots,N\}, Nh = T$, where $N$ is a positive integer and $h$ the step size. We replace the charge $\tilde{q} : [0,T] \to M$, the current $\tilde{v} : [0,T] \to T_{\tilde{q}}M$, and the flux linkage $\tilde{p} : [0,T] \to T_{\tilde{q}}^*M$ by their discrete versions $\tilde{q}_d : \{t_k\}_{k=0}^N \to M$, $\tilde{v}_d : \{t_k\}_{k=0}^N \to T_{\tilde{q}}M$ and $\tilde{p}_d : \{t_k\}_{k=0}^N \to T_{\tilde{q}}^*M$, where we view $\tilde{q}_k = \tilde{q}_d(kh)$, $\tilde{v}_k = \tilde{v}_d(kh)$, and $\tilde{p}_k = \tilde{p}_d(kh)$ as an approximation to $\tilde{q}(kh)$, $\tilde{v}(kh)$, and $\tilde{p}(kh)$, respectively.

### 4.1. Forward Euler

We replace the reduced Lagrange-d'Alembert-Pontryagin principle with a discrete version

$$\delta\left\{h\sum_{k=0}^{N-1}\left(\mathcal{L}^M(\tilde{q}_k,\tilde{v}_k)+\left\langle\tilde{p}_k,\frac{\tilde{q}_{k+1}-\tilde{q}_k}{h}-\tilde{v}_k\right\rangle\right)\right\}+h\sum_{k=0}^{N-1}f_L^M(\tilde{q}_k,\tilde{v}_k,t_k)\delta\tilde{q}_k=0, \tag{20}$$

where in (20) the time derivative $\dot{\tilde{q}}(t)$ is approximated by the forward difference operator and the force evaluated at the left point.

For discrete variations $\delta\tilde{q}_k$ that vanish in the initial and final points as $\delta\tilde{q}_0=\delta\tilde{q}_N=0$ and discrete variations $\delta\tilde{v}_k$ and $\delta\tilde{p}_k$ this gives

$$\begin{aligned}&\left\langle\frac{\partial\mathcal{L}^M}{\partial\tilde{v}}(\tilde{q}_0,\tilde{v}_0)-\tilde{p}_0,\delta\tilde{v}_0\right\rangle+\sum_{k=1}^{N-1}\left[\left\langle\frac{\partial\mathcal{L}^M}{\partial\tilde{q}}(\tilde{q}_k,\tilde{v}_k)-\frac{1}{h}(\tilde{p}_k-\tilde{p}_{k-1})+f_L^M(\tilde{q}_k,\tilde{v}_k,t_k),\delta\tilde{q}_k\right\rangle\left\langle\delta\tilde{p}_{k-1},\frac{\tilde{q}_k-\tilde{q}_{k-1}}{h}-\tilde{v}_{k-1}\right\rangle\right.\\&\left.+\left\langle\frac{\partial\mathcal{L}^M}{\partial\tilde{v}}(\tilde{q}_k,\tilde{v}_k)-\tilde{p}_k,\delta\tilde{v}_k\right\rangle\right]+\left\langle\delta\tilde{p}_{N-1},\frac{\tilde{q}_N-\tilde{q}_{N-1}}{h}-\tilde{v}_{N-1}\right\rangle=0.\end{aligned} \tag{21}$$

This leads to the discrete reduced constrained Euler–Lagrange equations

$$\frac{\partial\mathcal{L}^M}{\partial\tilde{v}}(\tilde{q}_0,\tilde{v}_0)=\tilde{p}_0, \tag{22a}$$

$$\left.\begin{aligned}&\tfrac{\partial\mathcal{L}^M}{\partial\tilde{q}}(\tilde{q}_k,\tilde{v}_k)-\tfrac{1}{h}(\tilde{p}_k-\tilde{p}_{k-1})+f_L^M(\tilde{q}_k,\tilde{v}_k,t_k)=0\\&\tfrac{\tilde{q}_k-\tilde{q}_{k-1}}{h}=\tilde{v}_{k-1}\\&\tfrac{\partial\mathcal{L}^M}{\partial\tilde{v}}(\tilde{q}_k,\tilde{v}_k)=\tilde{p}_k\end{aligned}\right\}k=1,\dots,N-1, \tag{22b}$$

$$\frac{\tilde{q}_N-\tilde{q}_{N-1}}{h}=\tilde{v}_{N-1}. \tag{22c}$$

For the Lagrangian defined in (13) and the Lagrangian forces defined in (14), this results in

$$\tilde{p}_0=K_2^TLK_2\tilde{v}_0, \tag{23a}$$

$$\left.\begin{aligned}&\tfrac{\tilde{p}_k-\tilde{p}_{k-1}}{h}=K_2^T(-CK_2\tilde{q}_k-\mathrm{diag}(R)K_2\tilde{v}_k+u_s(t_k))\\&\tfrac{\tilde{q}_k-\tilde{q}_{k-1}}{h}=\tilde{v}_{k-1}\\&K_2^TLK_2\tilde{v}_k=\tilde{p}_k\end{aligned}\right\}k=1,\dots,N-1, \tag{23b}$$

$$\frac{\tilde{q}_N-\tilde{q}_{N-1}}{h}=\tilde{v}_{N-1}. \tag{23c}$$

This gives the following update rule: For given $(\tilde{q}_0,\tilde{v}_0)$, use (23a) to compute $\tilde{p}_0$. Then, use the iteration scheme

$$\begin{pmatrix}I&0&0\\0&K_2^TLK_2&-I\\hK_2^TCK_2&hK_2^T\mathrm{diag}(R)K_2&I\end{pmatrix}\begin{pmatrix}\tilde{q}_k\\\tilde{v}_k\\\tilde{p}_k\end{pmatrix}=\begin{pmatrix}I&hI&0\\0&0&0\\0&0&I\end{pmatrix}\begin{pmatrix}\tilde{q}_{k-1}\\\tilde{v}_{k-1}\\\tilde{p}_{k-1}\end{pmatrix}+\begin{pmatrix}0\\0\\hK_2^T\end{pmatrix}u_s(t_k)\quad\text{for } k=1,\dots,N, \tag{24}$$

to compute $\tilde{q}_1,\dots,\tilde{q}_N,\tilde{v}_1,\dots,\tilde{v}_N$ and $\tilde{p}_1,\dots,\tilde{p}_N$.

**Proposition 2.** *System (24) is uniquely solvable if the matrix $K_2^T(L+h\mathrm{diag}(R))K_2$ is regular.*

**Proof.** System (24) is uniquely solvable if the iteration matrix $A=\begin{pmatrix}I&0&0\\0&K_2^TLK_2&-I\\hK_2^TCK_2&hK_2^T\mathrm{diag}(R)K_2&I\end{pmatrix}$ has zero nullspace. For $Az=0$ with $z=(\tilde{q},\tilde{v},\tilde{p})$, we have (i) $\tilde{q}=0$, (ii) $\tilde{p}=K_2^TLK_2\tilde{v}$, (iii) $hK_2^TCK_2\tilde{q}+hK_2^T\mathrm{diag}(R)K_2\tilde{v}+\tilde{p}=0$. Substituting (i) and (ii) in (iii) gives $K_2^T(L+h\mathrm{diag}(R))K_2\tilde{v}=0$. Thus, $z=0$ is the unique solution of $Az=0$ iff $K_2^T(L+h\mathrm{diag}(R))K_2$ has zero nullspace. □

### 4.2. Backward Euler

If we approximate the time derivative $\dot{\tilde{q}}(t)$ by the backward difference operator rather than by the forward difference operator as

$$\delta\left\{h\sum_{k=1}^{N}\left(\mathcal{L}^M(\tilde{q}_k,\tilde{v}_k)+\left\langle\tilde{p}_k,\frac{\tilde{q}_k-\tilde{q}_{k-1}}{h}-\tilde{v}_k\right\rangle\right)\right\}+h\sum_{k=1}^{N}f_L^M(\tilde{q}_k,\tilde{v}_k,t_k)\delta\tilde{q}_k=0, \tag{25}$$

with discrete variations $\delta\tilde{q}_k$ that vanish in the initial and final points as $\delta\tilde{q}_0=\delta\tilde{q}_N=0$ and discrete variations $\delta\tilde{v}_k$ and $\delta\tilde{p}_k$, we obtain

$$\begin{aligned}&\left\langle\delta\tilde{p}_1,\frac{\tilde{q}_1-\tilde{q}_0}{h}-\tilde{v}_1\right\rangle+\left\langle\frac{\partial\mathcal{L}^M}{\partial\tilde{v}}(\tilde{q}_1,\tilde{v}_1)-\tilde{p}_1,\delta\tilde{v}_1\right\rangle+\sum_{k=2}^{N}\left[\left\langle\delta\tilde{p}_k,\frac{\tilde{q}_k-\tilde{q}_{k-1}}{h}-\tilde{v}_k\right\rangle\right.\\&\left.+\left\langle\frac{\partial\mathcal{L}^M}{\partial\tilde{q}}(\tilde{q}_{k-1},\tilde{v}_{k-1})-\frac{1}{h}(\tilde{p}_k-\tilde{p}_{k-1})+f_L^M(\tilde{q}_{k-1},\tilde{v}_{k-1},t_{k-1}),\delta\tilde{q}_{k-1}\right\rangle+\left\langle\frac{\partial\mathcal{L}^M}{\partial\tilde{v}}(\tilde{q}_k,\tilde{v}_k)-\tilde{p}_k,\delta\tilde{v}_k\right\rangle\right]=0.\end{aligned} \tag{26}$$

This gives a slight, but in this case significant, modification for the Euler–Lagrange equations as

$$\frac{\tilde{q}_1-\tilde{q}_0}{h}=\tilde{v}_1, \tag{27a}$$

$$\frac{\partial\mathcal{L}^M}{\partial\tilde{v}}(\tilde{q}_1,\tilde{v}_1)=\tilde{p}_1, \tag{27b}$$

$$\left.\begin{aligned}&\tfrac{\partial\mathcal{L}^M}{\partial\tilde{q}}(\tilde{q}_{k-1},\tilde{v}_{k-1})-\tfrac{1}{h}(\tilde{p}_k-\tilde{p}_{k-1})+f_L^M(\tilde{q}_{k-1},\tilde{v}_{k-1},t_{k-1})=0\\&\tfrac{\tilde{q}_k-\tilde{q}_{k-1}}{h}=\tilde{v}_k\\&\tfrac{\partial\mathcal{L}^M}{\partial\tilde{v}}(\tilde{q}_k,\tilde{v}_k)=\tilde{p}_k\end{aligned}\right\}k=2,\dots,N. \tag{27c}$$

Note that in contrast to the variational scheme (22) that consists of an explicit update for the charges $q$ and an implicit update for the fluxes $p$, we now get an implicit scheme for $q$ and an explicit scheme for $p$. In particular, for the Lagrangian (13) and the forces (14), we obtain the following update rule: for given $(\tilde{q}_0,\tilde{v}_0)$ compute $\tilde{p}_0$ via $\tilde{p}_0=K_2^TLK_2\tilde{v}_0$. Then, use the iteration scheme

$$\begin{pmatrix}I&-hI&0\\0&K_2^TLK_2&-I\\0&0&I\end{pmatrix}\begin{pmatrix}\tilde{q}_k\\\tilde{v}_k\\\tilde{p}_k\end{pmatrix}=\begin{pmatrix}I&0&0\\0&0&0\\-hK_2^TCK_2&-hK_2^T\mathrm{diag}(R)K_2&I\end{pmatrix}\begin{pmatrix}\tilde{q}_{k-1}\\\tilde{v}_{k-1}\\\tilde{p}_{k-1}\end{pmatrix}+\begin{pmatrix}0\\0\\hK_2^T\end{pmatrix}u_s(t_{k-1})\quad\text{for } k=1,\dots,N, \tag{28}$$

to compute $\tilde{q}_1,\dots,\tilde{q}_N,\tilde{v}_1,\dots,\tilde{v}_N$ and $\tilde{p}_1,\dots,\tilde{p}_N$.

**Proposition 3.** *System (28) is uniquely solvable if the matrix $K_2^TLK_2$ is regular.*

**Proof.** System (28) is uniquely solvable if the iteration matrix $A=\begin{pmatrix}I&-hI&0\\0&K_2^TLK_2&-I\\0&0&I\end{pmatrix}$ has zero nullspace. For $Az=0$ with $z=(\tilde{q},\tilde{v},\tilde{p})$, we have (i) $\tilde{q}=h\tilde{v}$, (ii) $\tilde{p}=K_2^TLK_2\tilde{v}$, (iii) $\tilde{p}=0$. Thus, $z=0$ is the unique solution of $Az=0$ iff $K_2^TLK_2$ has zero nullspace. □

Proposition 3 says that whenever the KCL cancels the degeneracy of the system, the backward Euler scheme is applicable, whereas the forward Euler scheme is applicable to a wider class of circuit systems (cf. Proposition 2) for $h$ sufficiently large. The resulting variational Euler schemes (22) and (27) consisting of a combination of implicit and explicit updates are first order variational integrators. The construction of higher order implicit schemes (e.g., variational partitioned Runge–Kutta (VPRK) methods along the lines of [31]) allows the simulation of arbitrary circuits. As an example, we present in the following a variational integrator based on the implicit midpoint rule.

### 4.3. Implicit midpoint rule

We introduce internal stages $\widetilde{Q}_k,\widetilde{P}_k,\widetilde{V}_k,\ k=1,\dots,N-1$ that are given on a second time grid $\Delta\tau=\{\tau_k=(k+\frac{1}{2})h\,|\,k=0,\dots,N-1\}$ and define the internal stage vectors $\widetilde{Q}_d:\{\tau_k\}_{k=0}^{N-1}\to M,\widetilde{V}_d:\{\tau_k\}_{k=0}^{N-1}\to T_{\tilde{q}}M$ and $\widetilde{P}_d:\{\tau_k\}_{k=0}^{N-1}\to T_{\tilde{q}}^*M$ to be $\widetilde{V}_k=\tilde{v}(t_k+\frac{1}{2}h),\widetilde{Q}_k=\tilde{q}_k+\frac{1}{2}h\widetilde{V}_k,\widetilde{P}_k=\frac{\partial\mathcal{L}^M}{\partial\tilde{v}}(\widetilde{Q}_k,\widetilde{V}_k)$. The approximations at the nodes are then determined by the internal stages via $\tilde{q}_{k+1}=\tilde{q}_k+h\widetilde{V}_k$ and $\tilde{p}_{k+1}=\tilde{p}_k+h\frac{\partial\mathcal{L}^M}{\partial\tilde{q}}(\widetilde{Q}_k,\widetilde{V}_k)$.

By taking variations $\delta\tilde{q}_k,\delta\widetilde{Q}_k,\delta\tilde{p}_k,\delta\widetilde{P}_k,\delta\widetilde{V}_k$ for the following discrete Lagrange-d'Alembert-Pontryagin principle with $\delta q_N=0$ but free $\delta\tilde{q}_0$ and initial value $\tilde{q}^0$

$$\delta\left\{h\sum_{k=0}^{N-1}\left(\mathcal{L}^M(\widetilde{Q}_k,\widetilde{V}_k)+\left\langle\widetilde{P}_k,\frac{\widetilde{Q}_k-\tilde{q}_k}{h}-\frac{1}{2}\widetilde{V}_k\right\rangle+\left\langle\tilde{p}_{k+1},\frac{\tilde{q}_{k+1}-\tilde{q}_k}{h}-\widetilde{V}_k\right\rangle\right)+\langle\tilde{p}_0,\tilde{q}_0-\tilde{q}^0\rangle\right\}+h\sum_{k=0}^{N-1}f_L^M(\widetilde{Q}_k,\widetilde{V}_k,\tau_k)\delta\widetilde{Q}_k=0 \tag{29}$$

gives

$$\sum_{k=0}^{N-1}\left[\left\langle \frac{\partial \mathcal{L}^M}{\partial \tilde{q}}(\widetilde{Q}_k,\widetilde{V}_k)+\frac{\widetilde{P}_k}{h}+f_L^M(\widetilde{Q}_k,\widetilde{V}_k,\tau_k),\delta\widetilde{Q}_k\right\rangle+\left\langle \frac{\partial \mathcal{L}^M}{\partial \tilde{v}}(\widetilde{Q}_k,\widetilde{V}_k)-\frac{1}{2}\widetilde{P}_k-\tilde{p}_{k+1},\delta\widetilde{V}_k\right\rangle\right.$$
$$\left.+\left\langle \delta\widetilde{P}_k,\frac{\widetilde{Q}_k-\tilde{q}_k}{h}-\frac{1}{2}\widetilde{V}_k\right\rangle+\left\langle \delta\tilde{p}_{k+1},\frac{\tilde{q}_{k+1}-\tilde{q}_k}{h}-\widetilde{V}_k\right\rangle+\left\langle \frac{-\widetilde{P}_k-\tilde{p}_{k+1}+\tilde{p}_k}{h},\delta\tilde{q}_k\right\rangle\right]+\langle\delta\tilde{p}_0,\tilde{q}_0-\tilde{q}^0\rangle=0. \tag{30}$$

The Euler–Lagrange equations are

$$\frac{\partial \mathcal{L}^M}{\partial \tilde{q}}(\widetilde{Q}_k,\widetilde{V}_k)+\frac{\widetilde{P}_k}{h}+f_L^M(\widetilde{Q}_k,\widetilde{V}_k,\tau_k)=0, \tag{31a}$$
$$\frac{\partial \mathcal{L}^M}{\partial \tilde{v}}(\widetilde{Q}_k,\widetilde{V}_k)-\frac{1}{2}\widetilde{P}_k-p_{k+1}=0, \tag{31b}$$
$$\frac{\widetilde{Q}_k-\tilde{q}_k}{h}-\frac{1}{2}\widetilde{V}_k=0, \tag{31c}$$
$$\frac{\tilde{q}_{k+1}-\tilde{q}_k}{h}-\widetilde{V}_k=0, \tag{31d}$$
$$-\widetilde{P}_k-\tilde{p}_{k+1}+\tilde{p}_k=0,\quad k=0,\dots,N-1, \tag{31e}$$
$$\tilde{q}_0-\tilde{q}^0=0. \tag{31f}$$

By eliminating $\widetilde{P}_k$ by Eq. (31e) together with $\widetilde{V}_k=\tilde{v}_{k+\frac{1}{2}}, \widetilde{Q}_k=\frac{\tilde{q}_k+\tilde{q}_{k+1}}{2}$ (which follows from (31c) and (31d)) and $\tau_k=\frac{t_k+t_{k+1}}{2}=t_{k+\frac{1}{2}}$ leads to the iteration scheme

$$\tilde{p}_{k+1}=\tilde{p}_k+h\frac{\partial \mathcal{L}^M}{\partial \tilde{q}}\left(\frac{\tilde{q}_k+\tilde{q}_{k+1}}{2},\tilde{v}_{k+\frac{1}{2}}\right)+hf_L^M\left(\frac{\tilde{q}_k+\tilde{q}_{k+1}}{2},\tilde{v}_{k+\frac{1}{2}},t_{k+\frac{1}{2}}\right), \tag{32a}$$
$$\tilde{q}_{k+1}=\tilde{q}_k+h\tilde{v}_{k+\frac{1}{2}}, \tag{32b}$$
$$\frac{\tilde{p}_k+\tilde{p}_{k+1}}{2}=\frac{\partial \mathcal{L}^M}{\partial \tilde{v}}\left(\frac{\tilde{q}_k+\tilde{q}_{k+1}}{2},\tilde{v}_{k+\frac{1}{2}}\right),\quad k=0,\dots,N-1. \tag{32c}$$

**Remark 6.** The integrator (32) is equivalent to a Runge–Kutta scheme with coefficients $a=\frac{1}{2}, b=1, c=\frac{1}{2}$ (implicit midpoint rule integrator) applied to the corresponding Hamiltonian system.

For the circuit case with Lagrangian (13) and forces (14), we start with given $(\tilde{q}_0,\tilde{p}_0)$ to solve iteratively for $(\tilde{q}_{k+1},\tilde{v}_{k+\frac{1}{2}},\tilde{p}_{k+1})$, $k=0,\dots,N-1$ for given $u_s(t)$ using the scheme

$$\begin{pmatrix} I & -hI & 0\\ 0 & K_2^TLK_2 & -\frac{1}{2}I\\ \frac{1}{2}hK_2^TCK_2 & hK_2^T\mathrm{diag}(R)K_2 & I\end{pmatrix}\begin{pmatrix}\tilde{q}_{k+1}\\ \tilde{v}_{k+\frac{1}{2}}\\ \tilde{p}_{k+1}\end{pmatrix}=\begin{pmatrix} I & 0 & 0\\ 0 & 0 & \frac{1}{2}I\\ -\frac{1}{2}hK_2^TCK_2 & 0 & I\end{pmatrix}\begin{pmatrix}\tilde{q}_k\\ \tilde{v}_{k-\frac{1}{2}}\\ \tilde{p}_k\end{pmatrix}+\begin{pmatrix}0\\0\\hK_2^T\end{pmatrix}u_s\left(t_{k+\frac{1}{2}}\right) \tag{33}$$

for $k=0,\dots,N-1$.

**Remark 7.** The discrete current $\tilde{v}_{k+\frac{1}{2}}$, which plays the role of the algebraic variable in the continuous setting, is only approximated between two discrete time nodes $t_k$ and $t_{k+1}$. Also, note that $\tilde{v}_{k-\frac{1}{2}}$ is not explicitly used for the computation of $(\tilde{q}_{k+1},\tilde{v}_{k+\frac{1}{2}},\tilde{p}_{k+1})$ (which corresponds to a zero column in the matrix of the right hand side of (33)). This means that the computation of the magnitudes at time point $t_{k+1}$ depends only on the discrete magnitudes within the time interval $[t_k,t_{k+1}]$, which is characteristic for a one-step scheme. In particular, $\tilde{v}_{-\frac{1}{2}}(k=0)$ is a pseudo-variable that is not used.

**Proposition 4.** *System (33) is uniquely solvable if the matrix $K_2^T(2L+h\mathrm{diag}(R)+\frac{1}{2}h^2C)K_2$ is regular.*

**Proof.** System (33) is uniquely solvable if the iteration matrix $A=\begin{pmatrix} I & -hI & 0\\ 0 & K_2^TLK_2 & -\frac{1}{2}I\\ \frac{1}{2}hK_2^TCK_2 & hK_2^T\mathrm{diag}(R)K_2 & I\end{pmatrix}$ has zero nullspace. For $Az=0$ with $z=(\tilde{q},\tilde{v},\tilde{p})$, we have (i) $\tilde{q}=h\tilde{v}$, (ii) $\tilde{p}=2K_2^TLK_2\tilde{v}$, (iii) $\frac{1}{2}hK_2^TCK_2\tilde{q}+hK_2^T\mathrm{diag}(R)K_2\tilde{v}+\tilde{p}=0$. Substituting (i) and (ii) in (iii) gives $K_2^T(2L+h\mathrm{diag}(R)+\frac{1}{2}h^2C)K_2\tilde{v}=0$. Thus, $z=0$ is the unique solution of $Az=0$ if $K_2^T(2L+h\mathrm{diag}(R)+\frac{1}{2}h^2C)K_2$ has zero nullspace. □

Note that for linear circuits, the condition given in Proposition 4 is satisfied for $h$ sufficiently large if the continuous system (18) has a unique solution.

**Remark 8** (*Condition numbers*). From Proposition 1, we see that the continuous reduced system (17) may be still degenerate due to the intrinsic degeneracy of the circuit topology and configuration. On the discrete side, both the forward Euler and the midpoint integrator show some regularization property: by perturbing $K_2^T L K_2$ in magnitude proportional to the time step size $h$, both integrators can render the degenerate continuous reduced system (17) into regular discrete systems (24) and (33), respectively. However, this regularization comes at the price of possible large condition numbers as explained in the following. The iteration matrices $A$ of the different schemes can be written as $A = A_0 + hE$ with $A_0 = \begin{pmatrix} I & 0 & 0 \\ 0 & K_2^T L K_2 & -I \\ 0 & 0 & I \end{pmatrix}$ and $E$ given by the respective iteration scheme. If the reduced system is regular (i.e., $K_2^T L K_2$ is non singular), $A_0$ is non singular with positive constant condition number $\kappa(A_0)$ and $\kappa(A)$ approaches a positive constant when the step size $h$ goes to zero (e.g., one can compute the singular values of the perturbed matrix $A_0 + hE$ using arguments from perturbation theory). In this case, all iteration schemes are well conditioned independent of the step size $h$. However, if the reduced system is degenerate, that is $K_2^T L K_2$ is singular, also $A_0$ is singular and the condition numbers of the forward Euler and the midpoint scheme grow reciprocally to the time step size $h$, that is $\kappa(A) \approx \mathcal{O}(1/h)$ for small $h$. When the circuit topology is fixed, the circuit's physical parameters are constants and the time step $h$ is also fixed, preconditioner can be precomputed and applied to the systems (24) and (33) to improve their numerical stabilities. Since this work mainly focuses on the theoretical aspects of variational integrators, we leave this stability issues for future work and assume thereafter no such issues in the subsequent discussion.

**Remark 9** (*Discussion on general DAE integration methods*). By deriving the discrete variational schemes, we constructed special integrators for the simulation of DAE systems. In general, integration methods for DAE systems can be divided into two main classes, namely one-step methods (such as implicit Runge–Kutta methods) and multi-step methods (such as BDF methods). These are typically well-suited for numerical solutions of index 1 DAE systems, while difficulties my arise for systems of higher index ([32]). Thus, index reduction techniques are applied to transform DAE systems of higher index to index 1 DAE systems via differentiation of the algebraic constraint. This comes with the drawback of violation of the algebraic constraint, which is no longer present during the numerical integration. To overcome this, several stabilization techniques have been proposed (for an overview see for example [32] and references therein). In geometric integration, variational and other geometric integrators such as Rattle and Shake [33] (which have been shown to be variational as well [1]) have been developed for the integration of DAE systems, where the algebraic part stems from the presence of holonomic or nonholonomic constraints. In this work, not only the presence of the KVL constraints but also the intrinsic degeneracy of the Lagrangian causes the differential–algebraic nature of the Euler–Lagrange equations. Thus, besides the KVL constraints, which are the holonomic constraints, also the primary constraints are part of the algebraic equations. The reduced formulation eliminates the holonomic constraints by choosing a new set of coordinates that parametrize the constraint KVL space, however, the primary constraints are still involved. To the best of our knowledge, the presented approach is the first one for the variational integration of DAE system resulting from primary constraints. Of course, general DAE integrators such as BDF methods or implicit Runge–Kutta methods, which do not rely on the geometric structure of the problem, do not distinguish between the origin of the algebraic equation. They can be applied as well. However, they do not preserve the geometric properties as demonstrated by means of numerical examples in Section 7.

## 5. Structure-preserving properties

In this section, we summarize the main structure-preserving properties of variational integrators (see for example [1]) and their interpretation for the case of electric circuits.

### 5.1. Symplecticity and preservation of momentum maps induced by symmetries

*Symplecticity*. In the case of conservative systems, the flow on $T^*Q$ of the Euler–Lagrange equations preserves the canonical symplectic form $\Omega = dq^i \wedge dp^i = \mathbf{d}\theta$ of the Hamiltonian system, where $\theta = p^i dq^i$ is the canonical one-form. Variational integrators are symplectic, that is the same property holds for the discrete flow of the discrete Euler–Lagrange equations; the canonical discrete symplectic form $\Omega = dq_0^i \wedge dp_0^i$ is exactly preserved for the discrete solution. Thus, in the case that the reduced formulation leads to a non-degenerate Lagrangian, there is a well-defined non-degenerate symplectic form, which is preserved by our iteration scheme. By using techniques from backward error analysis (see for example [33]), it can be shown that symplectic integrators also have good energy properties, that is for long-time integrations, there is no artificial energy growth or decay due to numerical errors. This can also be observed for our circuit examples in Section 7. In the case of linear LC circuits that involve a quadratic potential, a second order variational integrator, for example the midpoint variational integrator as derived in Section 4.3, exactly preserves the energy (magnetic plus electric energy).

*Conformal symplecticity*. In the presence of resistors, the system is dissipative and the symplectic form is not preserved anymore. However, in general, conformal symplecticity can be shown if the dissipative forces are uniform, that is the dissipation matrix is a scalar. Formally, let $\varphi_t$ denote the flow map of the Hamiltonian system with dissipation. Note that by assuming that $f_L^M = c\tilde{p}$, $c \in \mathbb{R}$, the Euler–Lagrange equations in (17) can also be derived by introducing the action integral

$$\mathfrak{S}(\tilde{q},\tilde{v},\tilde{p}) = \int_0^T \exp(ct)\left[\mathcal{L}^M(\tilde{q}(t),\tilde{v}(t)) + \left\langle \tilde{p}(t), \dot{\tilde{q}}(t) - \tilde{v}(t)\right\rangle\right] dt \tag{34}$$

and by taking variations as $\mathbf{d}\mathfrak{S}(\tilde{q},\tilde{v},\tilde{p})\cdot(\delta\tilde{q},\delta\tilde{v},\delta\tilde{p}) = 0$. Now we restrict $\mathfrak{S}$ to the space of pathwise unique solutions, which can be identified with the set of initial conditions. The restricted action can be expressed as $\hat{\mathfrak{S}} : TQ \oplus T^*Q \to \mathbb{R}$. One then computes

$$\mathbf{d}\hat{\mathfrak{S}}(\tilde{q}(0),\tilde{v}(0),\tilde{p}(0))\cdot(\delta\tilde{q}(0),\delta\tilde{v}(0),\delta\tilde{p}(0)) = \exp(ct)\langle\tilde{p},\delta\tilde{q}\rangle|_0^T. \tag{35}$$

These boundary terms define in local coordinates the one-form $\exp(ct)\theta$ on $T^*Q$. Computing $\mathbf{d}^2\hat{\mathfrak{S}}$ gives the conservation of $\exp(-ct)\Omega$ under the flow map, thus we have $(\varphi_t)^*\Omega = \exp(-ct)\Omega$ for all $t$. Note that for the case of the electric circuit, the condition $f_L^M = c\tilde{p}$ includes that $K_2^T\mathrm{diag}(R)K_2(K_2^TLK_2)^{-1}$ can be written as diagonal matrix $\mathrm{diag}(c)$ with diagonal entries $c$ by assuming that the reduced Lagrangian $\mathcal{L}^M$ is non-degenerate.

Now let $\varphi_h^N : T^*Q \to T^*Q$ denote $N$ steps of an integrator that approximates the flow map. The algorithm is conformally symplectic if $(\varphi_h^N)^*\Omega = \exp(-chN)\Omega$. This means that a discrete scheme that is conformally symplectic exactly preserves the rate of decay of the symplectic form. Consequently, one would expect that a conformally symplectic integrator would preserve the rate of energy decay much better than integrators, which are not conformally symplectic. In Section 7.2, we numerically show for an RLC circuit, that indeed the variational integrators constructed in Section 4 preserve the rate of energy decay much better than a Runge–Kutta or a BDF method. The proof of conformal symplecticity in the discrete case is analogous to that of Theorem 4.1 of [34].

*Preservation of momentum maps induced by symmetries* Noether's theorem states that momentum maps that are induced by symmetries in the system are preserved. More precisely, let $G$ be a Lie group acting on $Q$ by $\Phi : G\times Q \to Q$. We write $\Phi_g := \Phi(g,\cdot)$. The tangent lift of this action $\Phi^{TQ} : G\times TQ \to TQ$ is given by $\Phi_g^{TQ}(v_q) = T(\Phi_g)\cdot v_q$ with $v_q \in TQ$. The action is associated with a corresponding momentum map $J : TQ \to \mathfrak{g}^*$, where $\mathfrak{g}^*$ is the dual of the Lie algebra $\mathfrak{g}$ of $G$. The momentum map is defined by

$$\langle J(q,v),\xi\rangle = \left\langle \frac{\partial\mathcal{L}}{\partial v}, \xi_Q(q)\right\rangle = \langle p, \xi_Q(q)\rangle \quad \forall\xi\in\mathfrak{g},$$

where $\xi_Q$ is the infinitesimal generator of the action on $Q$, that is $\xi_Q(q) := \frac{d}{dt}|_{t=0}\Phi(\exp(t\xi),q)$ and $\exp : \mathfrak{g}\to G$ is the exponential function. A holonomic system that is described by a Lagrangian $\mathcal{L}$ and a holonomic constraint $h(q) = 0$ has a symmetry if the Lagrangian and the constraint are both invariant under the (lift of the) group action, that is $\mathcal{L}\circ\Phi_g^{TQ} = \mathcal{L}$ and $h\circ\Phi_g(q) = 0$ for all $g\in G$. Noether's theorem states that if the system has a symmetry, the corresponding momentum map is preserved. In presence of external forces, this statement is still true if the force is orthogonal to the group action. The discrete version of Noether's theorem [1] states that if the discrete Lagrangian has a symmetry, the corresponding momentum map is still preserved. The variational integrator based on this discrete Lagrangian is thus exactly momentum-preserving. For constrained and forced systems, the preservation still holds with the additional invariance and orthogonality conditions on constraints and forces analogous to the continuous case.

If we consider an electric circuit, we are faced with a constrained distribution given by the KCL and external forces due to resistors and voltage sources. The KCL are formulated on the tangent space; however, since these are linear, they are integrable, and the KCL can be formulated on the configuration space. Thus, in the following, we are able to apply the theory of holonomic systems to derive a preserved quantity for an eletrical circuit under some topology assumptions of the underlying graph.

**Proposition 5** (*Invariance of Lagrangian*). *The Lagrangian (6) of the unreduced system is invariant under the translation of $q_L$.*

**Proof.** Consider the group $G = \mathbb{R}^{n_L}$ with group element $g\in G$. Let $\Phi : G\times Q\to Q$ be the action of $G$ defined as $\Phi(g,q) = (q_L+g, q_C)$ for each $g\in G$ with tangent lift $\Phi^{TQ} : G\times TQ\to TQ, \Phi^{TQ}(g,(q,v)) = (q_L+g, q_C, q_R, q_V, v_L, v_C, v_R, v_V)$. Then, we have

$$\mathcal{L}\circ\Phi_g^{TQ}(q,v) = \frac{1}{2}\begin{pmatrix} v_L\\ v_C\\ v_R\\ v_V\end{pmatrix}^T L\begin{pmatrix} v_L\\ v_C\\ v_R\\ v_V\end{pmatrix} - \frac{1}{2}\begin{pmatrix} q_L+g\\ q_C\\ q_R\\ q_V\end{pmatrix}^T C\begin{pmatrix} q_L+g_L\\ q_C\\ q_R\\ q_V\end{pmatrix} = \frac{1}{2}v^TLv - \frac{1}{2}q^TCq = \mathcal{L}(q,v),$$

since $C = \mathrm{diag}\left(\frac{1}{C_1},\ldots,\frac{1}{C_n}\right)$ with the first $n_L$ diagonal elements being zero. □

**Assumption 1** (*Topology assumption*). *For every node $j$, $j = 1,\ldots,m$ in the circuit (except ground), the same amount of inductor branches connect inward and outward to node $j$.*

In particular, Assumption 1 implies that the sum of each row of $K_L^T$ is zero, that is $\sum_{j=1}^{n_L}(K_L^T)_{ij} = 0$ for $i = 1, \ldots, m$.

**Proposition 6** (*Invariance of distribution*). *Under Assumption 1, the KCL on configuration level are invariant under equal translation of $q_L$.*

**Proof.** The group element $g \in G$ that describes an equal translation of all components of $q_L$ can be expressed as $g = a\mathbf{1}$ with $a \in \mathbb{R}$ and $\mathbf{1}$ being a vector in $\mathbb{R}^{n_L}$ with each component 1. It follows that

$$K^T \circ \Phi_g(q) = K^T \begin{pmatrix} q_L + g \\ q_C \\ q_R \\ q_V \end{pmatrix} = K^T q + K_L^T g = K^T q + K_L^T \mathbf{1} a = K^T q,$$

since the sum of each row of $K_L^T$ is zero. □

**Proposition 7** (*Orthogonality of external force*). *The external force $f_L$ (8) is orthogonal to the action of the group $G = \mathbb{R}^{n_L}$ being translations of $q_L$.*

**Proof.** Let $\xi \in \mathfrak{g} = \mathbb{R}^{n_L}$ be an element of the Lie algebra. For the group action $\Phi_g(q) = (q_L + g, q_C, q_R, q_V)$, the infinitesimal generator can be calculated as

$$\xi_Q(q) = \frac{d}{dt}\Big|_{t=0} \Phi_{\exp t\xi}(q) = \frac{d}{dt}\Big|_{t=0} (q_L + \exp t\xi, q_C, q_R, q_V) = (\xi, 0, 0, 0).$$

Thus, we have

$$\langle f_L, \xi_Q(q)\rangle = \langle -\mathrm{diag}(R)v + \mathrm{diag}(\mathcal{E})u, \xi_Q(q)\rangle = 0,$$

since $\mathrm{diag}(R)$ and $\mathrm{diag}(\mathcal{E})$ have zero entries in the first $n_L$ lines and columns. □

**Theorem 2** (*Preservation of flux*). *Under Assumption 1, the sum of all inductor fluxes in the electric circuit described by the Lagrangian (6), the external forces (8), and the KCL is preserved.*

**Proof.** From Proposition 5–7 we know that the Lagrangian and the KCL are invariant under the group action $\Phi_g(q) = (q_L + g, q_C, q_R, q_V)$ with $g \in G = \mathbb{R}^{n_L}$ and the external force $f_L$ is orthogonal to this group action. It follows with Noether's theorem that the induced momentum map is preserved by the flow of the system. For the momentum map, we calculate

$$\langle J(q, v), \xi\rangle = \left\langle \frac{\partial \mathcal{L}}{\partial v}, \xi_Q(q) \right\rangle = \frac{\partial \mathcal{L}}{\partial v_i} \xi_Q^i(q) = \frac{\partial \mathcal{L}}{\partial v_{L_i}} \xi^i.$$

Thus, the preserved momentum map is $J(q, v) = \sum_{i=1}^{n_L} p_{n_{L_i}}$, which is the sum of the fluxes of all inductors in the circuit. □

**Remark 10** (*Proof based on Euler–Lagrange equations*). An alternative proof can be derived based on the Euler–Lagrange equations in the following way. From (12a), we have

$$\dot{p}_L = K_L \lambda.$$

For the time derivative of the sum of all inductors, it follows that

$$\frac{d}{dt}\sum_{i=1}^{n_L} p_i = \sum_{i=1}^{n_L} \dot{p}_i = \sum_{i=1}^{n_L}\sum_{j=1}^{m} (K_L)_{ij}\lambda_j = \sum_{j=1}^{m} \lambda_j \sum_{i=1}^{n_L} (K_L)_{ij} = 0,$$

since with Assumption 1, we have $0 = \sum_{i=1}^{n_L}(K_L^T)_{ji} = \sum_{i=1}^{n_L}(K_L)_{ij}$ for $j = 1, \ldots, m$. Thus, $\sum_{i=1}^{n_L} p_i$ is preserved.

**Remark 11** (*Momentum map for reduced system*). Also, for the reduced system described by the Lagrangian (13), the same momentum map can be computed by considering the group action $\Phi_{\tilde{g}}(\tilde{q}) = \tilde{q} + \tilde{g}$ with the group element $\tilde{g} \in \widetilde{G} \subset \mathbb{R}^{n-m}$ defined as $\tilde{g} = K_2^+ \begin{pmatrix} g \\ 0 \end{pmatrix}$ with $K_2^+$ being the well-defined pseudo-inverse of $K_2$.

**Lemma 1** (*Preserved momentum map*). *For any linear circuit that is described by the Lagrangian (6) the external forces (8), and the KCL, the momentum map defined by $\eta^T \frac{\partial \mathcal{L}}{\partial v}$ with $\eta \in ker(K_L^T)$ is preserved.*

**Proof.** By using the Euler–Lagrange equations, we see immediately

$$\frac{d}{dt}\eta^T \frac{\partial \mathcal{L}}{\partial v} = \eta^T \dot{p} = \eta^T K_L \lambda = 0,$$

since $\eta^T \in ker(K_L^T) \perp im(K_L) \ni K_L\lambda$ and thus, $\eta^T \frac{\partial \mathcal{L}}{\partial v} = const.$ □

The discrete Lagrangian system that includes constraints and forces introduced in Section 4 inherits the same symmetry and orthogonality property as the continuous system. Due to the discrete Noether theorem, the resulting variational integrators exactly preserves the sum of inductor fluxes under Assumption 1 (compare Section 7.4 for a numerical example).

### 5.2. Frequency spectrum

As can be observed in numerical examples (see Section 7), the frequency spectrum of the discrete solutions is much better preserved by using variational integrators rather than other integrators.

We want to analytically demonstrate this phenomenon by means of a simple harmonic 1d oscillator. Assume that the curves $(q(t), p(t))$ on $[0, T]$ describe the oscillatory behavior of the system. Consider the discrete solution $\{(q_k, p_k)\}_{k=0}^N$ defined on the discrete time grid $\{t_k\}_{k=0}^n$ with $t_0 = 0, t_N = T$ and $h = t_{k+1} - t_k$ that is obtained from the one-step update scheme $(q_{k+1}, p_{k+1})^T = A(q_k, p_k)^T$, $k = 0, \ldots, N-1$, where $A \in \mathbb{R}^{2,2}$ depends on the constant time step $h$. As known from variational integrator theory [1], the discrete solution $\{(q_k, p_k)\}_{k=0}^N$ converges to the solution $(q(t), p(t))$ for decreasing $h$. Since this solution is oscillating and due to the convergence of the scheme, at least one eigenvalue $\lambda_1$ of $A$ has to be complex (with nonzero imaginary part) for a small enough time step $h$. Since $A \in \mathbb{R}^{2,2}$, the second eigenvalue $\lambda_2$ has to be complex conjugate to the first one. Thus, the corresponding eigenvectors are linearly independent and $A$ is diagonalizable as $A = QVQ^{-1}$ with $V = \mathrm{diag}(\lambda_1, \lambda_2)$. With the coordinate transformation $(x_k, y_k)^T = Q^{-1}(q_k, p_k)^T$ we have $(x_{k+1}, y_{k+1})^T = V(x_k, y_k)^T$, that is $x_{k+1} = \lambda_1 x_k$ and $y_{k+1} = \lambda_2 y_k$.

We demonstrate the preservation of the frequency spectrum for the 1d oscillator in two steps: (i) We show that for a convergent scheme the update matrix $A$ has two eigenvalues both of norm 1 if and only if the update scheme is symplectic. (ii) We show that methods defined by matrices with norm 1 eigenvalues preserve the frequency spectrum defined on different time spans.

(i) "⇐": Assume that the scheme defined by $A$ is symplectic, then $\det(A) = 1$ (see for example [35]). It follows with $\lambda_1$ complex conjugate to $\lambda_2$ $(\lambda_2 = \lambda_1^*)$: $1 = \det(Q) \cdot \det(V) \cdot \det(Q^{-1}) = \lambda_1 \cdot \lambda_2 = |\lambda_1|^2 = |\lambda_2|^2$ and thus $|\lambda_i| = 1, i = 1, 2$. "⇒": Assume that $A$ has two complex conjugate eigenvalues $\lambda_1 = \lambda_2^*$ with $|\lambda_1| = |\lambda_2| = 1$, that is we write $\lambda_1 = e^{i\theta}$ and $\lambda_2 = e^{-i\theta}$ with $\theta \in \mathbb{R}$ and $V = \mathrm{diag}(e^{i\theta}, e^{-i\theta})$. Note that $\theta$ depends on the constant time step $h$ that is used for the discretization. Let $J = \begin{pmatrix} 0 & 1 \\ -1 & 0 \end{pmatrix}$ be the canonical symplectic form and introduce the non-canonical symplectic form $\widetilde{J} = Q^T J Q$. We show that $V$ preserves $\widetilde{J}$, and therefore $A$ preserves $J$, that is $A$ is symplectic. Since $J$ is skew-symmetric with zero diagonal, $\widetilde{J}$ is of the form $\begin{pmatrix} 0 & \triangle \\ -\triangle & 0 \end{pmatrix}$ with $\triangle \in \mathbb{R}$. It follows that

$$V^T \widetilde{J} V = \begin{pmatrix} e^{i\theta} & 0 \\ 0 & e^{-i\theta} \end{pmatrix} \begin{pmatrix} 0 & \triangle \\ -\triangle & 0 \end{pmatrix} \begin{pmatrix} e^{i\theta} & 0 \\ 0 & e^{-i\theta} \end{pmatrix} = \begin{pmatrix} 0 & e^{i\theta} e^{-i\theta} \triangle \\ -e^{-i\theta} e^{i\theta} \triangle & 0 \end{pmatrix} = \begin{pmatrix} 0 & \triangle \\ -\triangle & 0 \end{pmatrix} = \widetilde{J}.$$

(ii) Suppose that the discrete values $x_1, x_2, \ldots, x_N$ determined by the update scheme $A$ are known, and admit the following discrete inverse Fourier transformation

$$x_k = \frac{1}{N} \sum_{n=1}^{N} \tilde{x}_n \exp\left(\frac{2\pi i}{N} kn\right),\ k = 1, \ldots, N.$$

Consider a sequence of discrete points $\{X_k\}_{k=1}^N$ that is shifted by one time step such that $X_k = x_{k+1} = \lambda_1 x_k,\ k = 1, \ldots, N$, that is $\{X_k\}_{k=1}^N$ approximates the solution on a later time interval than $\{x_k\}_{k=1}^N$. This admits the following discrete inverse Fourier transformation

$$X_k = \frac{1}{N} \sum_{n=1}^{N} \lambda_1 \tilde{x}_n \exp\left(\frac{2\pi i}{N} kn\right),\ k = 1, \ldots, N,$$

that is $\widetilde{X}_n = \lambda_1 \tilde{x}_n$. By the definition of the frequency spectrum, we have $\widetilde{X}_n^* \widetilde{X}_n = \tilde{x}_n^* \lambda_1^* \lambda_1 \tilde{x}_n = \tilde{x}_n^* |\lambda_1|^2 \tilde{x}_n = \tilde{x}_n^* \tilde{x}_n$, where the last equality relies on the symplecticity. By shifting the discrete solution arbitrary times, we see that the spectrum will be preserved using different time intervals for the frequency analysis. This means that, in particular for long-time integration, a frequency analysis on a later time interval yields the same results as on an earlier time interval, which we denote by *preservation of the frequency spectrum*. The analysis for $y$ follows analogously, and with the linear transformation $Q$ the same holds for $q$ and $p$. On the other hand, if $|\lambda_{ij}| \neq 1$, $i, j = 1, 2$ (such as for non-symplectic or non-convergent methods), the frequency spectrum will either shrink or grow unbounded.

Although the analysis was only performed for the simple case of a 1d harmonic oscillator (in particular statement (i) is restricted to this case), we believe that for higher-dimensional systems, a similar statement as in (ii) can also be shown, which is left for future work.

*Relation to numerical results* For the numerical computations in Section 7, we perform a frequency analysis in two different ways: Firstly, we calculate the frequency spectrum on different time subintervals of the overall time integration interval $[0,T]$. This is directly connected to the analytical result of frequency preservation: We can observe that the spectrum is independent on the specific time interval if a symplectic integrator is used; however, by using a non-symplectic method, the spectrum is damped if it is calculated on a later time interval. Secondly, we use a fixed time interval $[0,T]$ for the frequency analysis but use different time steps which results in different iteration matrices $A$. As we saw for the harmonic oscillator, the magnitude of the two eigenvalues is independent on the time step $h$ if a symplectic integrator is used, however, it might de- or increase for increasing $h$ for a non-symplectic method (e.g., if the explicit Euler method is used, the absolute value of the eigenvalues is $1+\mathcal{O}(h^2)$ and the frequency spectrum would grow for larger $h$).

## 6. Noisy circuits

In this section, we extend the constructed variational integrator to the simulation of noisy electric circuits for which noise is added to each edge of the circuit. Following the description in [10], in the stochastic setting, the constrained stochastic variational principle is

$$\delta\int_0^T \mathcal{L}(q(t),v(t))+\langle p(t),\dot q(t)-v(t)\rangle\,dt+\int_0^T f_L(q(t),v(t),t)\cdot\delta q(t)\,dt+\int_0^T \delta q(t)\cdot(\Sigma\circ dW_t)=0 \tag{36}$$

with constrained variations $\delta q\in\Delta_Q(q)$, where $\Sigma$ is a $n\times n$ matrix, usually constant and diagonal, which indicates the amplitude of noise at each edge, $W_t$ is a $n$-dimensional Brownian motion, and the last stochastic integral is in the sense of Stratonovich. This principle leads to the constrained stochastic differential equation

$$\frac{\partial\mathcal{L}}{\partial q}-\dot p+f_L+\Sigma\circ\frac{dW_t}{dt}\in\Delta_Q^0(q), \tag{37a}$$

$$dq=v\,dt, \tag{37b}$$

$$\frac{\partial\mathcal{L}}{\partial v}-p=0, \tag{37c}$$

$$K^Tv=0, \tag{37d}$$

where by (37a), we mean that we have $\int_0^T\left(\frac{\partial\mathcal{L}}{\partial q}dt-dp+f_L dt+\Sigma\circ dW_t\right)=\int_0^T\mathcal{X}(q)\,dt$ for a vector field $\mathcal{X}(q)\in\Delta_Q^0(q)$ for any $T$. Correspondingly, the reduced stochastic variational principle reads

$$\delta\int_0^T \mathcal{L}^M(\tilde q(t),\tilde v(t))+\left\langle\tilde p(t),\dot{\tilde q}(t)-\tilde v(t)\right\rangle dt+\int_0^T f_L^M(\tilde q(t),\tilde v(t),t)\cdot\delta\tilde q(t)\,dt+\int_0^T\delta\tilde q(t)\cdot(K_2^T\Sigma\circ dW_t)=0. \tag{38}$$

This results in the reduced stochastic Euler–Lagrange equations

$$\frac{\partial\mathcal{L}^M}{\partial\tilde q}dt-d\tilde p+f_L^M dt+K_2^T\Sigma\circ dW_t=0, \tag{39a}$$

$$d\tilde q=\tilde v\,dt, \tag{39b}$$

$$\frac{\partial\mathcal{L}^M}{\partial\tilde v}-\tilde p=0. \tag{39c}$$

To derive the discrete equations with noise, the Stratonovich integral is approximated by a discrete version. For simplicity, we present the equations for the forward Euler iteration scheme only. On the interval $[t_k,t_{k+1}]$ the integral $\int_{t_k}^{t_{k+1}}\delta\tilde q(t)\cdot(K_2^T\Sigma\circ dW_t)$ is approximated by the discrete expression $\delta\tilde q_k\cdot(K_2^T\Sigma)B^k$ with $B^k\sim\mathcal{N}(0,h)$, $k=0,\dots,N-1$ (see also [10]). In this way, we obtain the following reduced stochastic discrete variational principle

$$\delta\left\{h\sum_{k=0}^{N-1}\left(\mathcal{L}^M(\tilde q_k,\tilde v_k)+\left\langle\tilde p_k,\frac{\tilde q_{k+1}-\tilde q_k}{h}-\tilde v_k\right\rangle\right)\right\}+h\sum_{k=0}^{N-1}f_L^M(\tilde q_k,\tilde v_k,t_k)\delta\tilde q_k+\sqrt{h}\sum_{k=0}^{N-1}K_2^T\Sigma\xi_k\cdot\delta\tilde q_k=0, \tag{40}$$

where for each $k=0,\dots,N-1$, $\xi_k$ is a $n$-dimensional vector with entries being independent standard normal random variables. The discrete reduced stochastic Euler–Lagrange equations that give the symplectic forward Euler iteration scheme is then given by

$$\frac{\partial \mathcal{L}^M}{\partial \tilde{q}}(\tilde{q}_k, \tilde{v}_k) - \frac{1}{h}(\tilde{p}_k - \tilde{p}_{k-1}) + f_L^M(\tilde{q}_k, v_k, t_k) + \frac{1}{\sqrt{h}} K_2^T \Sigma \xi_k = 0$$
$$\frac{\tilde{q}_k - \tilde{q}_{k-1}}{h} = \tilde{v}_{k-1}$$
$$\frac{\partial \mathcal{L}^M}{\partial v}(\tilde{q}_k, \tilde{v}_k) = \tilde{p}_k, \quad k = 1, \ldots, N.$$

Different symplectic variational schemes (e.g., backward Euler or midpoint scheme) can be derived in the same way as in Section 4 with an appropriate discretization for the Stratonovich integral. In [10], it is shown that the stochastic flow of a stochastic mechanical system on $T^*Q$ preserves the canonical symplectic form almost surely (i.e., with probability one with respect to the noise). Furthermore, an extension of Noether's theorem says that in presence of symmetries of the Lagrangian, the corresponding momentum map is preserved almost surely.

## 7. Examples

In the following section, we demonstrate the variational integration scheme by means of simple circuit examples. The numerical results are compared with solutions resulting from standard modeling and simulation techniques from circuit theory. In particular, we compare the variational integrator results based on Lagrangian models with solutions obtained with a Runge–Kutta scheme of fourth order, as well with solutions obtained by applying Backward Differentiation Formula (BDF) methods to models derived using the Modified Nodal Analysis (MNA). Since we are interested in the preservation properties of the integrators for constant time stepping, we use a constant step size $h$ for all methods to ensure a fair comparison. Note that arbitrary step size control destroys the good long time behavior (see for example [33]) of symplectic integrators. Time adaptive symplectic schemes can be constructed using for example Sundman and Poincaré transformations (see [36]). These or similar methods have to be extended for the integration of electric circuits for a comparison with standard non symplectic adaptive time stepping schemes.

For all examples, we use the convention that the charge vector $q \in \mathbb{R}^n$ is ordered as $q = (q_L, q_C, q_R, q_V)$, and correspondingly the current, voltage, and linkage flux vectors, as well as the Kirchhoff Constraint and the Fundamental Loop matrix.

### 7.1. Short introduction to MNA

In most circuit simulators, the Modified Nodal Analysis (MNA) is used to assemble the system of equations. In the following, we present the standard modified nodal analysis. We follow the description in [37]. A more detailed description can be found, for example, in [37–39]. The MNA consists of three steps: 1. Apply the Kirchhoff Constraint Law to every node except the ground. 2. Insert the representation for the branch current of resistors, capacitors, and current sources. 3. Add the representation for inductors and voltage sources explicitly to the system.

The combination of Kirchhoff's laws and the characteristic equations of the different elements yields the system of differential and algebraic equations

$$K_C^T \dot{q}_C(K_C \hat{u}, t) + K_R^T g(K_R \hat{u}, t) + K_L^T v_L + K_V^T v_V + K_I^T v_I(K\hat{u}, \dot{q}_C(K_C\hat{u}, t), v_L, v_V, t) = 0, \tag{41a}$$
$$\dot{p}_L(v_L, t) - K_L \hat{u} = 0, \tag{41b}$$
$$u_V(K\hat{u}, \dot{q}_C(K_C\hat{u}, t), v_L, v_V, t) - K_V \hat{u} = 0, \tag{41c}$$

with node voltages $\hat{u}$, branch currents through voltage and flux controlled elements $v_V$ and $v_L$, voltage dependent charges through capacitors $q_C$, current dependent fluxes through inductors $p_L$, voltage dependent conductance $g$, and controlled current and voltage sources $v_I$ and $u_V$. System (41) can be rewritten in compact form as

$$A[d(x(t), t)]' + b(x(t), t) = 0, \tag{42}$$

with

$$x = \begin{bmatrix} \hat{u} \\ v_L \\ v_V \end{bmatrix}, \quad A = \begin{bmatrix} K_C^T & 0 \\ 0 & I \\ 0 & 0 \end{bmatrix}, \quad d(x,t) = \begin{bmatrix} q_C(K_C\hat{u}, t) \\ p_L(v_L, t) \end{bmatrix}$$

and the obvious definition of $b$. The prime $[d(x,t)]' = \frac{d}{dt}[d(x(t),t)]$ denotes differentiation with respect to time. Since the matrix $A\frac{\partial d(x,t)}{\partial x}$ might be singular, Eq. (42) is not an ordinary differential equation but of differential algebraic type. For a detailed description of the properties of these equations, we refer for example to [32].

The standard approach to numerically solving the system of Eqs. (42) is to apply implicit multistep methods for the time discretization, in particular lower-order BDF schemes or the trapezoidal rule. For a detailed description of these methods, we refer for example to [37,40]. The advantage of BDF methods is the low computational cost compared to implicit Runge–Kutta methods. However, they may have bad stability properties (cf. [37]) and, in particular, they are not symplectic.

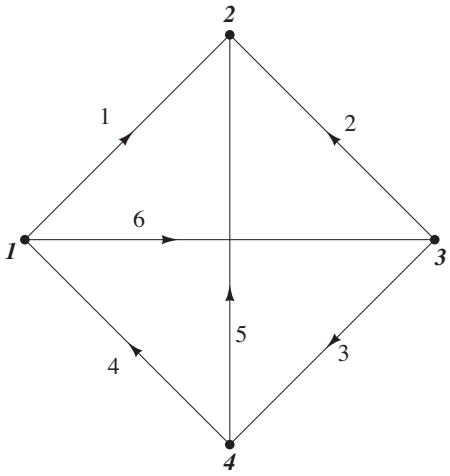


**Fig. 2.** Graph representation of a RLC circuit.

### 7.2. RLC circuit

Consider the graph consisting of four boundary edges and two diagonal edges of a square (see Fig. 2). On each edge of this graph, we have a pair of capacitor (with capacitance $C_i = 1, i = 1,\dots,6$) and inductor (with inductance $L_i = 1, i = 1,\dots,5$) except on one edge.[3] On this edge, there is only one capacitor which leaves a degenerate Lagrangian. The corresponding planar graph consists of $n = 6$ branches and $m + 1 = 4$ nodes, thus we have $l = 3$ meshes.

The matrix Kirchhoff Constraint matrix $K \in \mathbb{R}^{n,m}$ and the Fundamental Loop matrix $K_2 \in \mathbb{R}^{n,n-m}$ are (with the fourth node assumed to be grounded)

$$K = \begin{pmatrix} 1 & -1 & 0 \\ 0 & -1 & 1 \\ 0 & 0 & 1 \\ -1 & 0 & 0 \\ 0 & -1 & 0 \\ 1 & 0 & -1 \end{pmatrix}, \quad K_2 = \begin{pmatrix} 1 & 0 & -1 \\ 0 & -1 & 1 \\ 0 & 1 & 0 \\ 1 & 0 & 0 \\ -1 & 1 & 0 \\ 0 & 0 & 1 \end{pmatrix}. \tag{43}$$

The matrix $K_2^T L K_2$ is non-singular with $L = \mathrm{diag}(L_1,\dots,L_5,0)$; thus, the degeneracy of the system is eliminated by the constraints on the system, and all three variational integrators derived in Section 4, can be applied.

In Fig. 3(a), the oscillating behavior of the current on the first branch is shown (the currents on the other branches behave in a similar way). For the energy behavior of the LC circuit, we compare the exact solution with solutions obtained with the three different variational integrators, a Runge–Kutta method of fourth order, and a BDF method of second order. Since no resistor or voltage source is involved, this energy should be preserved. For the variational integrator based on the midpoint rule (VI), the energy is exactly preserved since the electric potential is only quadratic. For this relatively short integration time span, we observe that also the solution with the Runge–Kutta scheme (RK4) preserves the energy (the red solid, red dashed, and black dashed lines in Fig. 3(b) lie on top of each other). By using the forward (VI EFD, blue dotted) or backward Euler (VI EBD, blue dashed dotted) variational integrator, the energy oscillates around its real value, however, no dissipation or artificial growth of the energy occurs in contrast to the solution obtained by a BDF method (MNA BDF): Here, the energy rapidly decreases using a second order BDF method (see the magenta dashed dotted line in Fig. 3(b)). These results are based on a step size of $h = 0.1$. If the step size is increased to $h = 0.4$, a phase shifting of the currents that are computed with variational integrators is observed (which is a typical behavior observed for variational integrators) in contrast to solutions obtained by the Runge–Kutta scheme (see Fig. 4(a)).[4] However, considering the energy behavior shown in Fig. 4(b), energy is dissipating for the Runge–Kutta solution, whereas for the variational integrators it (its median, respectively) is preserved. The performance of the BDF method is even worse: The energy is dissipating very fast. This can also be observed considering the current in Fig. 4(a). The amplitude of the current oscillations is damped to almost zero after a certain integration time. Rather than increasing the step size, we use a small step size $h = 0.05$ and do a long-time integration. In Fig. 5, we see that the variational integrators still qualitatively preserve the energy, while the Runge–Kutta scheme slowly dissipates energy.

[3] The values for inductance and capacitance are just chosen for demonstration purpose of the variational integrator. For real circuits, the values are typically of different order, which results in a dynamical behavior on a different scale as in our numerical examples.

[4] Note that the Runge–Kutta method is of higher order (fourth order) than the variational integrators, and thus solution curves are of higher accuracy.

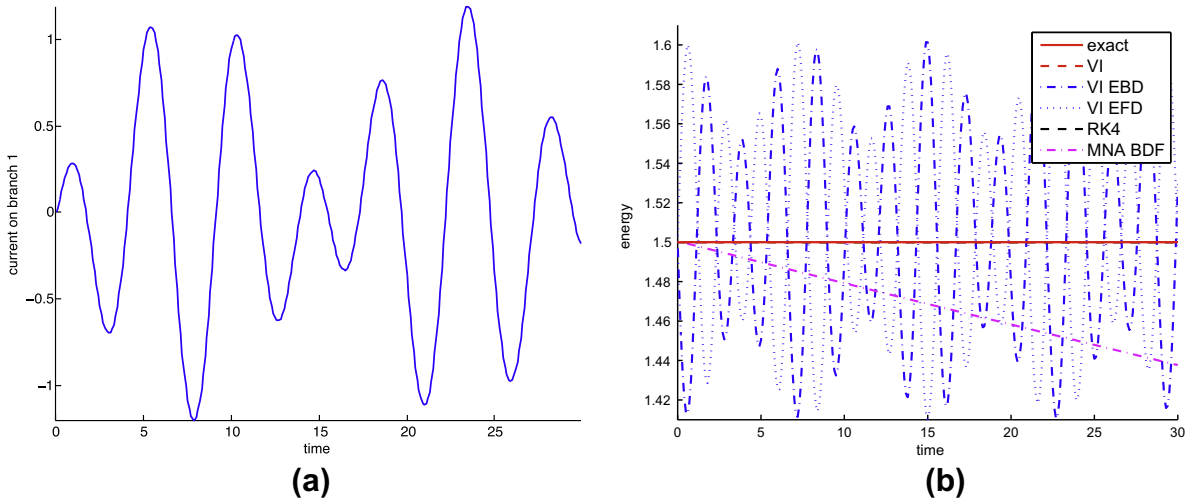


**Fig. 3.** LC circuit (no resistors) with step size $h = 0.1$. (a) The oscillating behavior of the current on the first branch is shown. (b) Comparison of the exact energy behavior (exact) and the numerical solution using the three different variational integrators, midpoint rule (VI), backward Euler (VI EBD), and forward Euler (VI EFD), a Runge–Kutta method of fourth order (RK), and a BDF method of second order based on MNA (MNA BDF). The energy is (qualitatively) preserved for VI, VI EBD, VI EFD, and RK. The lines of exact, VI, and RK lie on top of each other at energy level 1.5. The use of BDF leads to an artificial energy decay.

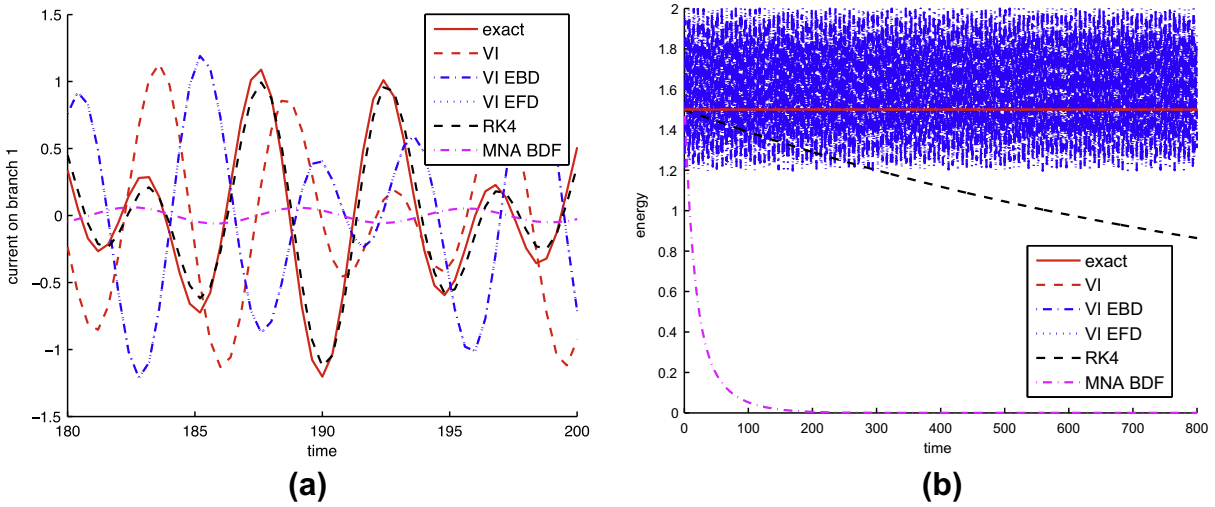


**Fig. 4.** LC circuit (no resistors) with step size $h = 0.4$. Comparison of the exact solution (exact) and the numerical solution using the three different variational integrators, midpoint rule (VI), backward Euler (VI EBD), and forward Euler (VI EFD), a Runge–Kutta method of fourth order (RK4), and a BDF method of second order based on MNA (MNA BDF). (a) The use of variational integrators (VI, VI EBD, VI EFD) leads to a phase shifting in the numerical solution of the current. With the BDF method, the oscillations are damped out. (b) The energy is (qualitatively) preserved for VI, VI EBD, and VI EFD. The lines of exact and VI lie on top of each other at energy level 1.5. The use of RK4 and BDF leads to an artificial energy decay.

We investigate the preservation properties even more by comparing the amplitude of the oscillating branch current and the corresponding spectrum in frequency domain for the different integration methods. The solution of the first branch current oscillates with two frequencies, $\omega_1 = 1$ and $\omega_2 = \sqrt{2}$. In Fig. 6, the branch current and the frequency spectrum for the discrete solution computed with two different step sizes ($h = 0.1, 0.4$) and different integrators are compared. For a bigger step size $h$, the amplitude of the oscillations and the spectrum of the higher frequency are artificially damped for the Runge–Kutta and the BDF method. However, using a variational integrator, the frequency is slightly shifted, but the spectrum is much better preserved. For $h = 0.4$, we compute the frequency spectrum for three different time intervals, $\left[0, \frac{T}{3}\right]$, $\left[\frac{T}{3}, \frac{2T}{3}\right]$, and $\left[\frac{2T}{3}, T\right]$. Corresponding to our analytical result regarding frequency preservation (see Section 5.2), we see in Fig. 7 that the frequency spectrum is the same independent on the integration time if a variational integrator is used. However, using the Runge–Kutta or BDF method it is damped if a time interval after a longer integration time is chosen.

In each branch of the circuit, we now add a small resistor with resistance $R_i = 0.001$, $i = 1, \ldots, 6$. Again, we compare the oscillating behavior and the energy behavior of the numerical solution obtained by different integrators. Due to the resistors,

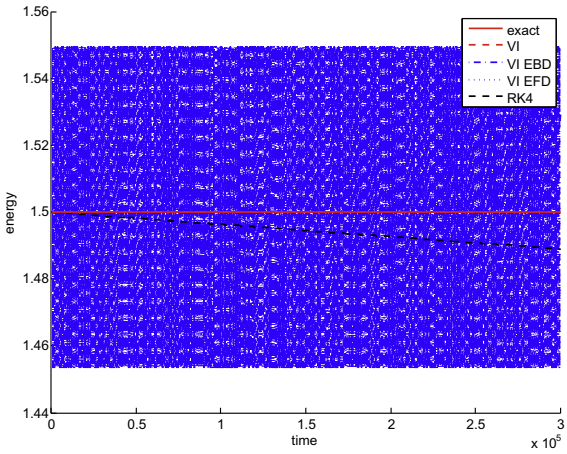


**Fig. 5.** LC circuit (no resistors) with step size $h = 0.05$. Comparison of the exact solution (exact) and the numerical solution using the three different variational integrators, midpoint rule (VI), backward Euler (VI EBD), and forward Euler (VI EFD), a Runge-Kutta method of fourth order (RK4). The long-time energy is (qualitatively) preserved for VI, VI EBD, and VI EFD. The lines of exact and VI lie on top of each other at energy value 1.5. The use of RK4 leads to an artificial energy decay.

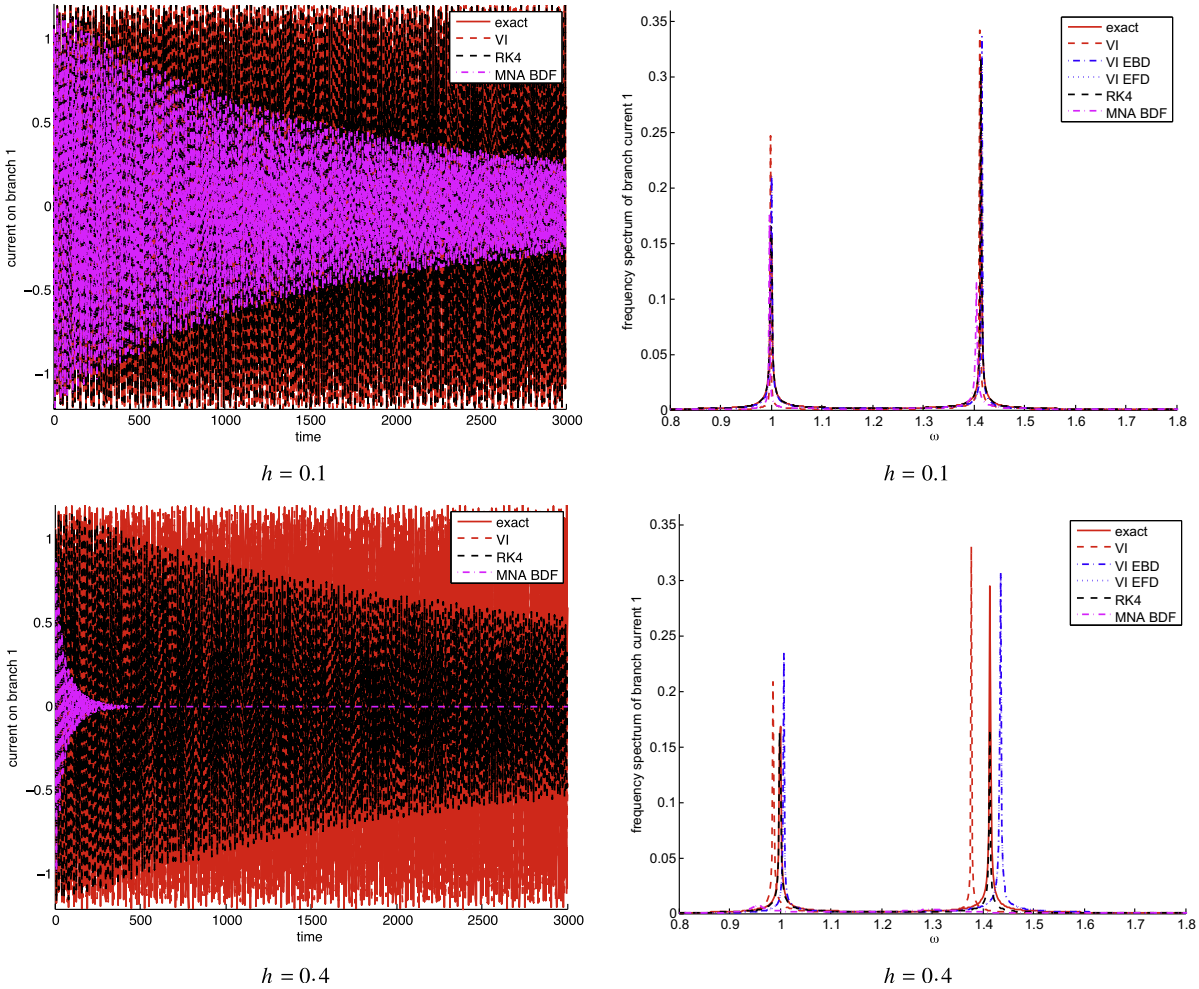


**Fig. 6.** Current of first branch of LC circuit (left) and corresponding frequency spectrum (right). Comparison of the exact solution (exact) and the numerical solution using the three different variational integrators, midpoint rule (VI), backward Euler (VI EBD), and forward Euler (VI EFD), a Runge-Kutta method of fourth order (RK4), and a BDF method of second order based on MNA (MNA BDF). For increasing step size $h$, the damping of the amplitude of the oscillations and of the higher frequency spectrum increases using RK4 and BDF. For VI, VI EBD, and VI EFD, the frequency is slightly shifted, but the spectrum and the current amplitude is much better preserved.

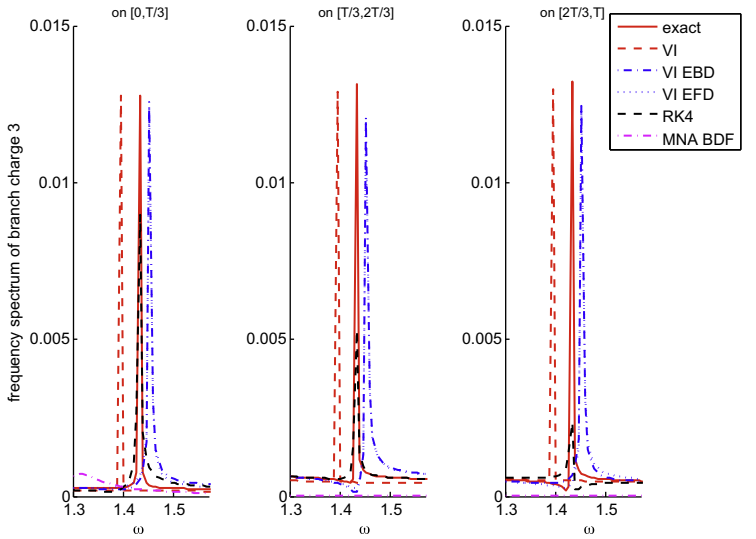


**Fig. 7.** Frequency spectrum of first branch current of LC circuit (no resistors) $h = 0.4$ computed on time interval $[0,T/3]$, $[T/3,2T/3]$, $[2T/3,T]$. Comparison of the exact solution (exact) and the numerical solution using the three different variational integrators, midpoint rule (VI), backward Euler (VI EBD), and forward Euler (VI EFD), a Runge-Kutta method of fourth order (RK4), and a BDF method of second order based on MNA (MNA BDF). Using RK4 and BDF the spectrum is damped for higher integration times and preserved using a variational integrator.

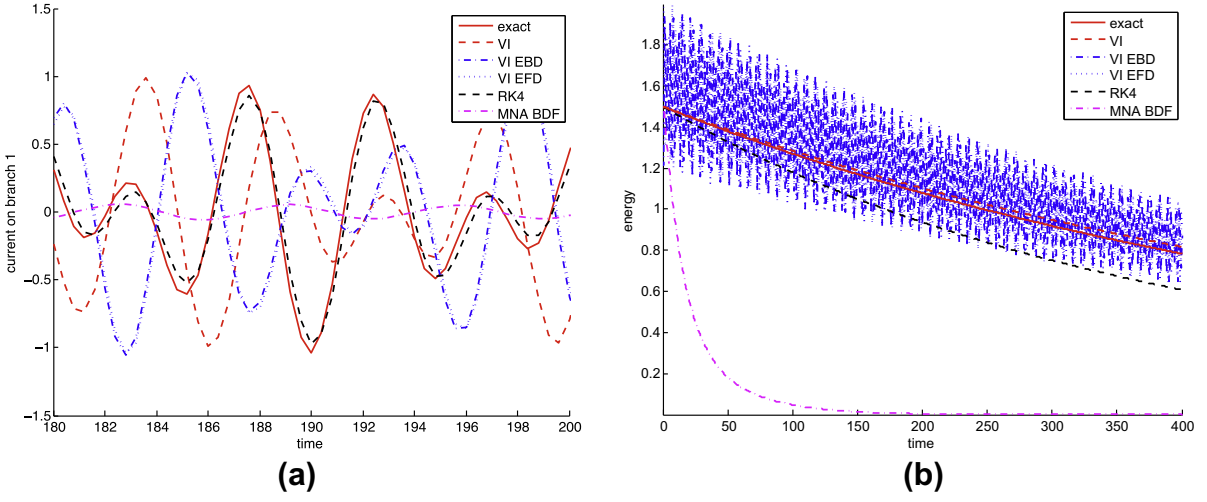


**Fig. 8.** LCR circuit (with resistors) with step size $h = 0.4$. Comparison of the exact solution (exact) and the numerical solution using the three different variational integrators, midpoint rule (VI), backward Euler (VI EBD), and forward Euler (VI EFD), a Runge-Kutta method of fourth order (RK4), and a BDF method of second order based on MNA (MNA BDF). a) The use of variational integrators (VI, VI EBD, VI EFD) leads to a phase shifting in the numerical solution of the current. With the BDF method, the oscillations are artificially damped out. b) The energy decay is much better preserved for VI, VI EBD, and VI EFD as for RK4 and BDF.

the energy in the system decays. The rate of energy decay is shown for the exact solution in Fig. 8(b). The variational integrator solution respects this energy decay much better than the Runge–Kutta and BDF scheme.

### 7.3. Oscillating LC circuit

As second example, we consider the LC circuit given in Fig. 9. It consists of two inductors with inductance $L_1 = 1$ and $L_2 = 1$ and two capacitors with capacitance $C_1 = 1$ and $C_2 = 10$ and thus has $n = 4$ branches and $m + 1 = 3$ nodes. The Kirchhoff Constraint matrix $K \in \mathbb{R}^{n,m}$ and the Fundamental Loop matrix $K_2 \in \mathbb{R}^{n,n-m}$ are (with the third node assumed to be grounded)

$$K = \begin{pmatrix} 1 & 0 \\ 0 & -1 \\ 0 & -1 \\ -1 & 1 \end{pmatrix}, \quad K_2 = \begin{pmatrix} 1 & 0 \\ 0 & 1 \\ 1 & -1 \\ 1 & 0 \end{pmatrix}. \tag{44}$$

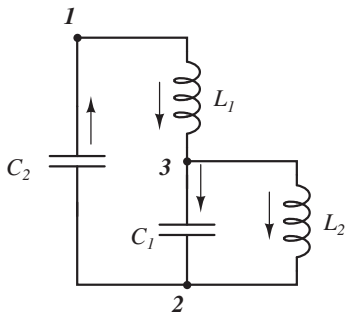


**Fig. 9.** Oscillating LC circuit.

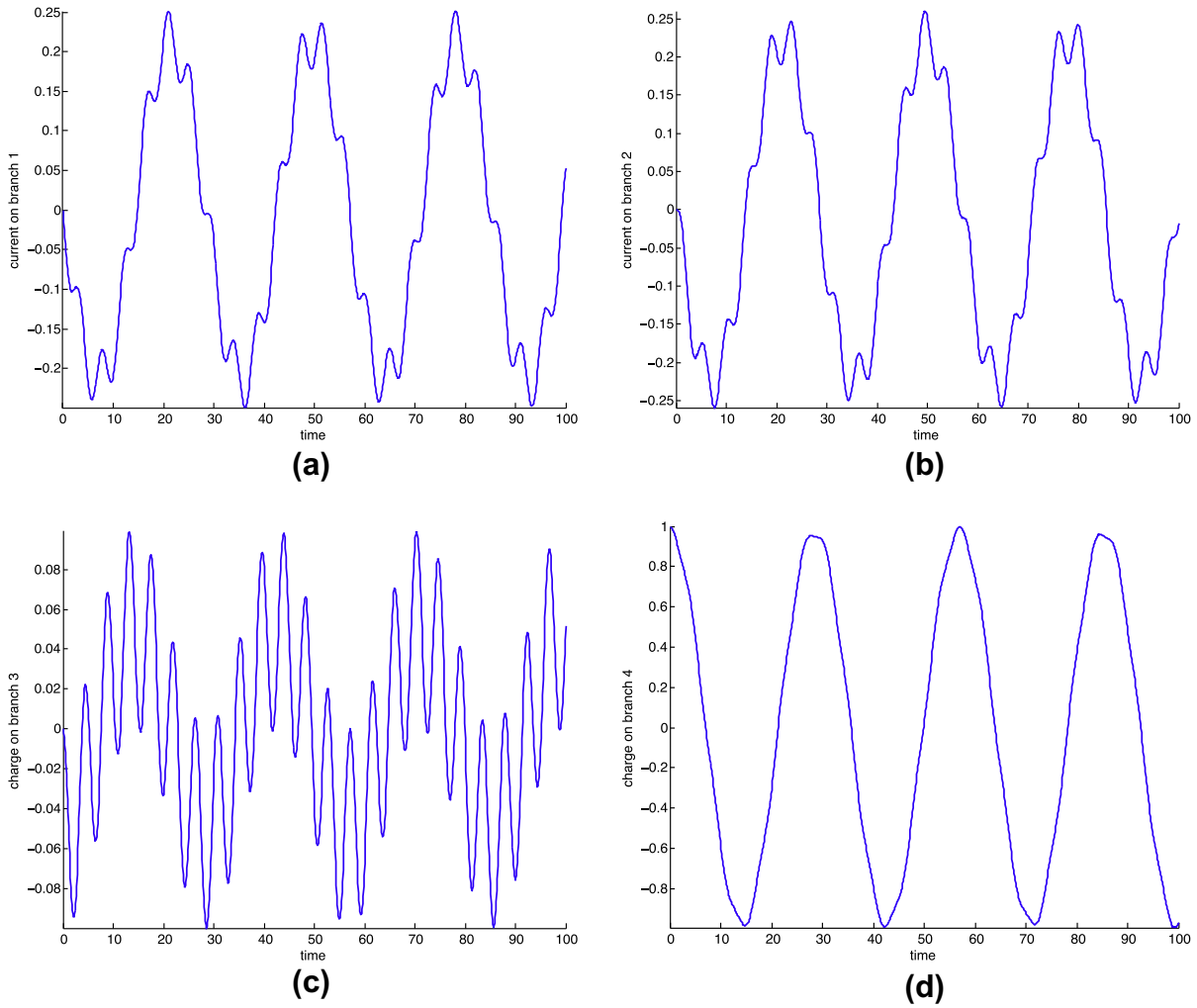


**Fig. 10.** LC circuit. (a) Current on inductor 1. (b) Current on inductor 2. (c) Charge on capacitor 1. (d) Charge on capacitor 2.

With $n_C = 2$ and $K_C = \begin{pmatrix} 0 & -1 \\ -1 & 1 \end{pmatrix}$ having full rank, we can follow from Proposition 1 that the reduced Lagrangian system is non-degenerate, that is all three variational integrators derived in Section 4 can be applied.

In Fig. 10, the oscillating behavior of the branch currents on the inductors (a)–(b) and of the branch charges on the capacitors (c)–(d) is depicted. For a long-time simulation, we compare the exact energy behavior of the LC circuit with the energy

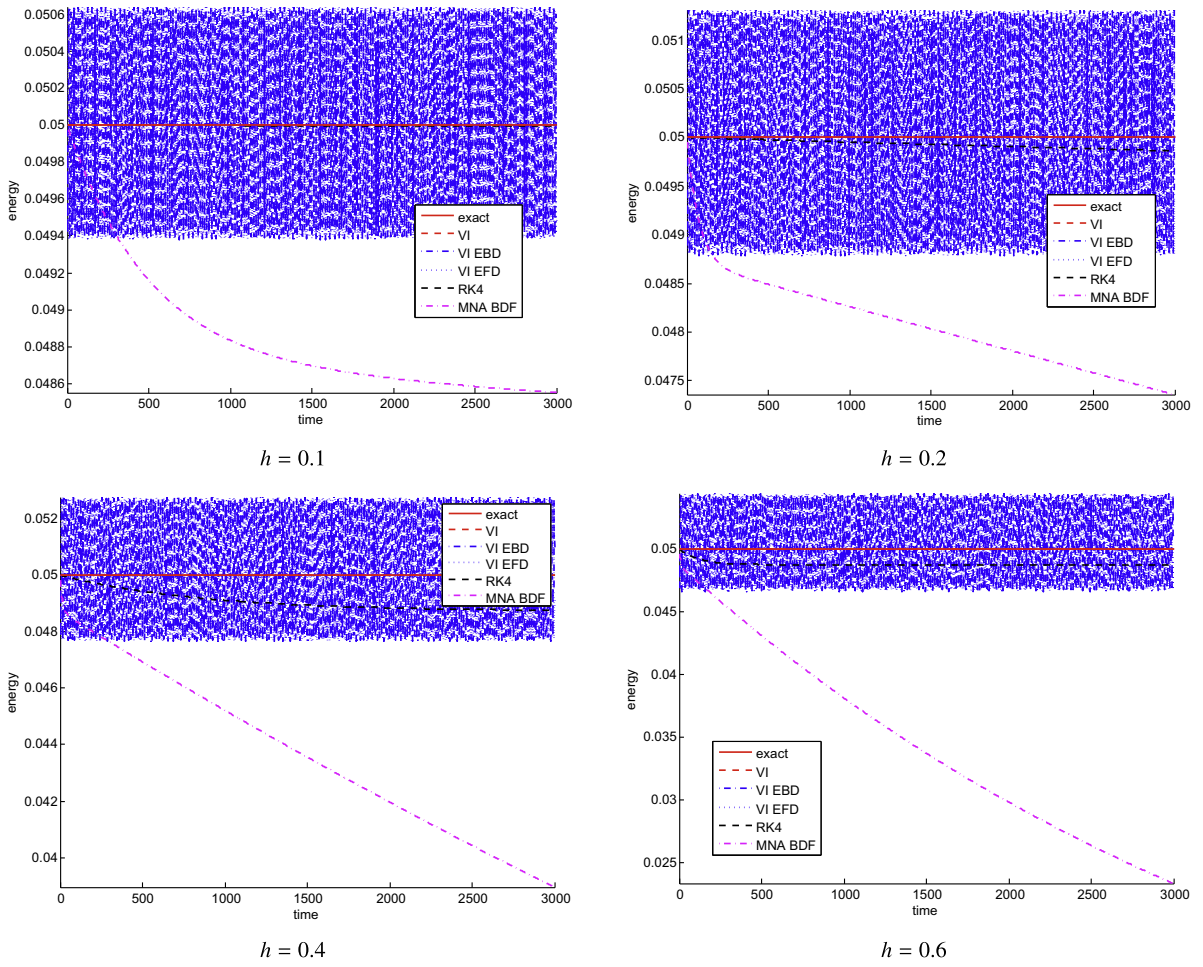


**Fig. 11.** Energy of oscillating LC circuit: Solutions obtained with the midpoint variational integrator exactly preserve the energy (VI) independent on the step size $h$. The energy computed with the forward (VI EFD) and backward (VI EBD) Euler variational integrators oscillates around the real energy value without dissipation or artificial growth. For solutions obtained with a second order BDF method (BDF MNA), the energy dissipates due to numerical errors. The solution of the Runge–Kutta scheme (RK4) dissipate energy, but seems to converge to lower constant energy value.

behavior of the solution obtained with the three different variational integrators (VI, VI EBD, VI EFD), a Runge–Kutta method of fourth order (RK4), and a BDF method of second order based on MNA (BDF MNA). As for the previous example, independent on the step size $h$, the energy is exactly preserved using VI based on midpoint rule, whereas the solutions using the Euler VI oscillate around the real energy value without dissipation or artificial growth of the energy (see Fig. 11). Using the BDF method, the energy rapidly decreases for increasing time step $h$. The solution of the Runge–Kutta scheme shows a similar decreasing energy behavior for the step size $h = 0.1, 0.2, 0.4$. However, for a step size of $h = 0.6$, the energy seems to converge to a constant value that is not the exact energy value, but slightly lower. This might be due to the fact that the amplitude of the first lower frequency is almost preserved and only the amplitude corresponding to the higher frequency is damped out for increasing integration time, as shown in Fig. 12 for different time spans and a step size of $h = 0.6$. The same property is reflected by the plots in the frequency domain in Fig. 13 for $h = 0.4$, where for increasing integration time the spectrum of the high frequency ($\omega_2 \approx 1.43$) is damped for the Runge–Kutta and BDF method and preserved using a symplectic method. This phenomenon is also confirmed by the frequency spectrum plot in Fig. 14 for different step sizes. As for the previous example, the spectrum that corresponds to the higher frequency is damped out for higher step sizes $h$ for the BDF and the Runge–Kutta method.

### 7.4. LC transmission line

To demonstrate the momentum map preservation properties of the variational integrator, we consider the LC transmission line that consists of a chain of inductors and capacitors as illustrated in Fig. 15. The matrix Kirchhoff Constraint matrix $K \in \mathbb{R}^{n,m}$ and the Fundamental Loop matrix $K_2 \in \mathbb{R}^{n,n-m}$ are (with the third node assumed to be grounded),

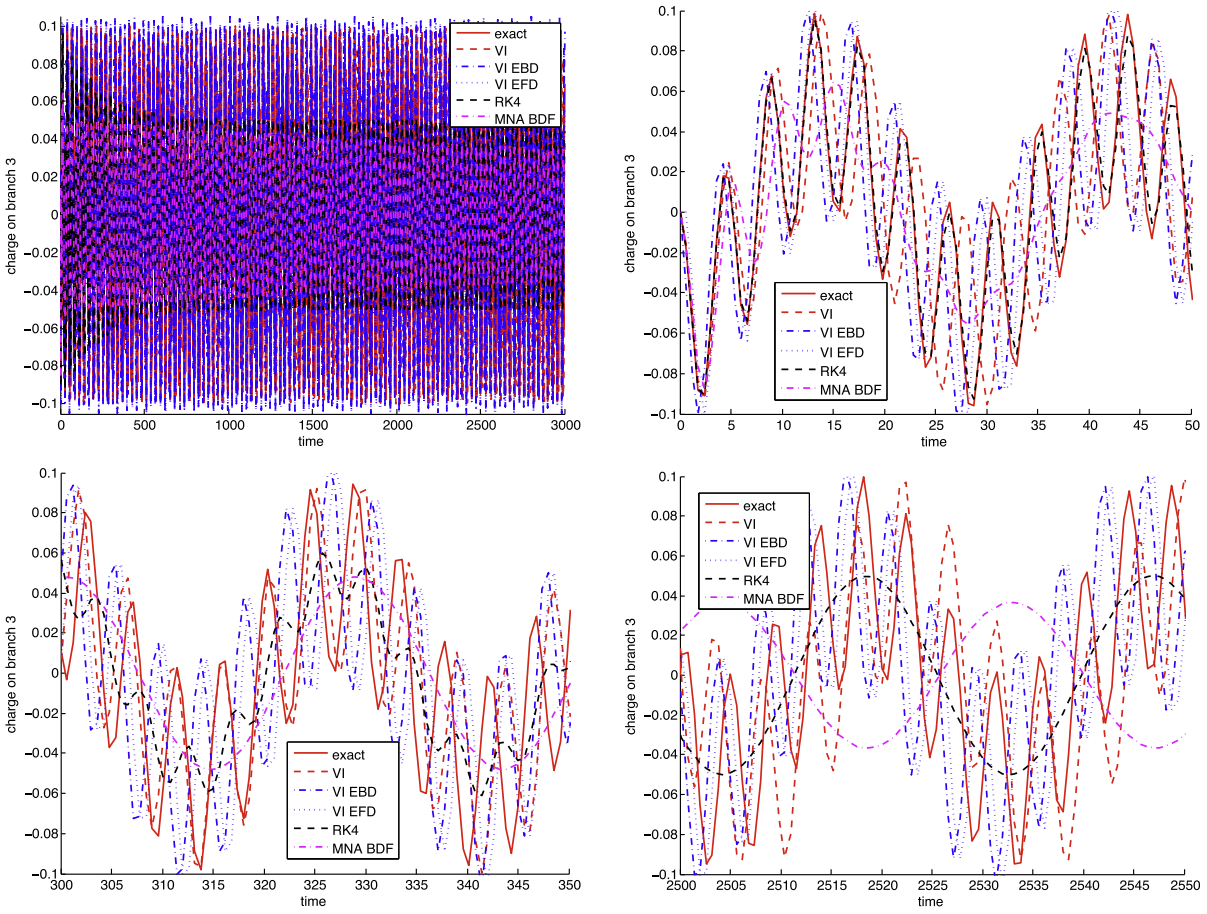


**Fig. 12.** Charge on capacitor 1 of LC circuit ($h = 0.6$). Comparison of the exact solution (exact) and the numerical solution using the three different variational integrators, midpoint rule (VI), backward Euler (VI EBD), and forward Euler (VI EFD), a Runge–Kutta method of fourth order (RK4), and a BDF method of second order based on MNA (MNA BDF). For the variational integrators the amplitudes for low and high frequencies are preserved. Using the Runge–Kutta method, the amplitude corresponding to the high frequency is damped out for increasing integration time whereas the amplitude of the lower one seems to be preserved. Using the BDF method, the amplitudes of both frequencies are damped.

$$K = \begin{pmatrix} -1 & 0 \\ 1 & -1 \\ 0 & 1 \\ 1 & 0 \\ 0 & 1 \end{pmatrix}, \quad K_2 = \begin{pmatrix} 1 & 0 & 0 \\ 0 & 1 & 0 \\ 0 & 0 & 1 \\ 1 & -1 & 0 \\ 0 & 1 & -1 \end{pmatrix}.$$

With $n_C = 2$ and $K_C = \begin{pmatrix} 1 & 0 \\ 0 & 1 \end{pmatrix}$ having full rank, we can follow from Proposition 1 that the reduced Lagrangian system is non-degenerate. For this circuit, the topology Assumption 1 is satisfied, that is all nodes except ground have exactly one branch connected and inward and outward to the node. Thus, from Theorem 2 we have that the sum of the inductor fluxes $p_{L_1} + p_{L_2} + p_{L_3}$ is a conserved quantity. This can be also seen from the variational simulation results depicted in Fig. 16.

### 7.5. Validation on the stochastic variational integrator

Consider the stochastic differential equation

$$dx = Axdt + \bar{\Sigma} dW_t, \tag{45}$$

where $\bar{\Sigma}$ is a $n$-by-$m$ matrix, not necessarily full rank, $x = (x_1, x_2, \ldots, x_n) \in \mathbb{R}^n, A \in \mathbb{R}^{n,n}$ and $W_t$ is an $m$-dimensional Brownian motion (with independent components). A common way to verify the quality of a numerical solution is to consider statistical moments of the solution; in particular, we focus on the expectation and the variance, that is $\mathbb{E}(x(t))$ and $\mathbb{D}(x(t)) = \mathbb{E}(x(t))^2 - (\mathbb{E}(x(t)))^2$.

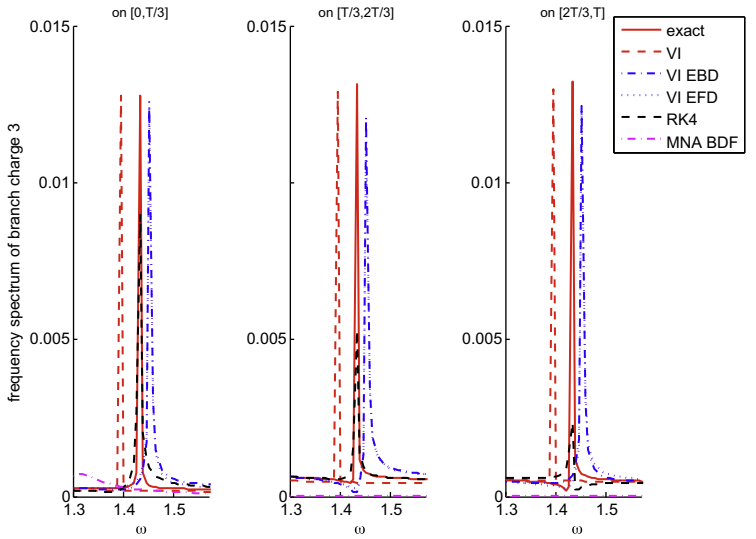


**Fig. 13.** Frequency spectrum of charge on capacitor 1 of LC circuit ($h = 0.4$) computed on time interval $[0, T/3]$, $[T/3, 2T/3]$, $[2T/3, T]$. Comparison of the exact solution (exact) and the numerical solution using the three different variational integrators, midpoint rule (VI), backward Euler (VI EBD), and forward Euler (VI EFD), a Runge–Kutta method of fourth order (RK4), and a BDF method of second order based on MNA (MNA BDF). Using RK4 and BDF the spectrum is damped for higher integration times and preserved using a variational integrator.

On the analytical side, by Ito's formula (see for example [41]) we have with $B(t) = \exp(At)$

$$\mathbb{E}(x(t)) = B(t)x(0), \tag{46a}$$

$$\mathbb{D}(x(t)) = \int_0^t B(\tau)\bar{\Sigma}\bar{\Sigma}^T B(\tau)^T d\tau. \tag{46b}$$

The expectation and the variance can always be computed if $A$ and $\bar{\Sigma}$ are given. For big systems, however, such a mundane computation is quite complex. On the numerical side, we run an ensemble of simulations (of total number $M$), all starting from the same initial condition but for each simulation an independent set of noise (i.e., different $\xi_k$) is used. The ensemble are indicated by $x^1(t), x^2(t), \ldots, x^M(t)$ where for any $j$, $x^j(t) = (x_1^j(t), x_2^j(t), \ldots, x_n^j(t))$ is a vector. We compute the empirical moments by

$$\bar{\mathbb{E}}(x(t)) \approx \frac{1}{M}\sum_{j=1}^{M} x^j(t), \tag{47a}$$

$$\bar{\mathbb{D}}(x(t)) \approx \frac{1}{M}\sum_{j=1}^{M} (x^j(t))^2 - \frac{1}{M^2}\left(\sum_{j=1}^{M} x^j(t)\right)^2. \tag{47b}$$

The numerical method is validated if for large enough $M$ the empirical moments (47) are close to the analytical ones (46).

In our setting, we can rewrite the reduced stochastic Euler–Lagrange Eqs. (39) in the form of (45) with $x = (\tilde{q}, \tilde{p}) \in \mathbb{R}^{2(n-m)}$, $\bar{\Sigma} = \begin{pmatrix} 0 & 0 \\ 0 & K_2^T\Sigma \end{pmatrix} \in \mathbb{R}^{2(n-m),2n}$, and the obvious definition of $A \in \mathbb{R}^{2(n-m),2(n-m)}$ with $\Sigma \in \mathbb{R}^{n,n}$ and $K_2 \in \mathbb{R}^{n,n-m}$. The analytical variance matrix $\mathbb{D}((\tilde{q}(t), \tilde{p}(t)) \in \mathbb{R}^{2(n-m),2(n-m)}$ for the reduced system can now be calculated using Eq. (46b). The corresponding variance matrix for the full system can then be calculated as

$$\mathbb{D}(q(t), p(t)) = \begin{pmatrix} K_2 & 0 \\ 0 & K_2 \end{pmatrix} \mathbb{D}(\tilde{q}(t), \tilde{p}(t)) \begin{pmatrix} K_2^T & 0 \\ 0 & K_2^T \end{pmatrix} \in \mathbb{R}^{2n,2n}.$$

As a demonstration, we calculate the empirical and analytical moments for the circuit introduced in Section 7.3. For the experiments throughout this section, we defined $\Sigma$ as 4-by-4 diagonal matrix with diagonal entries $\Sigma_{jj} = 0.01, j = 1, \ldots 4$. The step size is $h = 0.1$, the integration time for each simulation is $T = 30$, and we start with the initial conditions $\tilde{q}_0 = (1, 0)$, $\tilde{v}_0 = (0, 0)$, and $\tilde{p}_0 = (0, 0)$. The empirical averages are calculated over an ensemble of $M = 100000$ independent simulations.

The analytical variance of $p_{L_1}$ and $p_{L_2}$, that is the fifth and sixth diagonal elements of the variance matrix in the full system, are plotted as functions of time (see Fig. 17, red dotted line). Notice that $p_{L_1}$ and $p_{L_2}$ in our case are just the currents through inductor branch 1 and 2, the inductances are $L_1 = L_2 = 1$. The result using the stochastic variational integrator is also shown in Fig. 17 (blue solid line). Both function shapes and ranges agree very well. In particular, all the little bumps in the variance

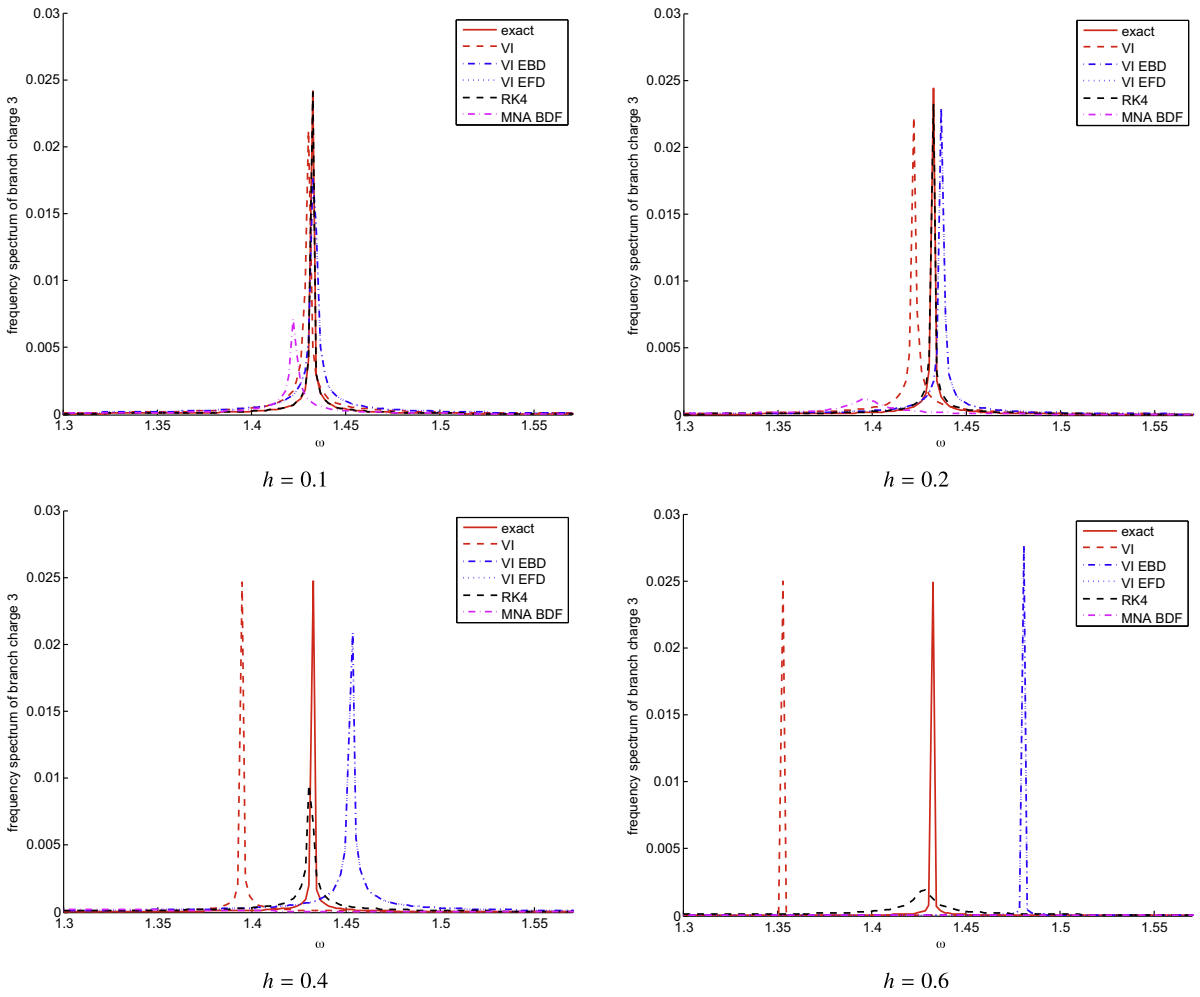


**Fig. 14.** Frequency spectrum of charge on capacitor 1 of LC circuit. Comparison of the exact solution (exact) and the numerical solution using the three different variational integrators, midpoint rule (VI), backward Euler (VI EBD), and forward Euler (VI EFD), a Runge–Kutta method of fourth order (RK4), and a BDF method of second order based on MNA (MNA BDF). For increasing step size $h$, the damping of the higher frequency spectrum increases using RK4 and BDF. For VI, VI EBD, and VI EFD, the frequency is slightly shifted, but the spectrum is much better preserved.

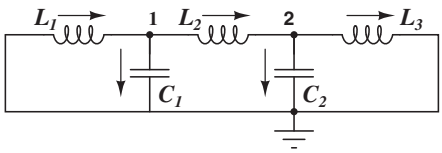


**Fig. 15.** LC transmission line.

that are subtly different are approximated correctly. This classical test serves as an evidence that the stochastic integration works fine.

### 7.6. Multiscale integration with FLAVORS

When the circuit exhibits behavior in two time scales, our integrators can be FLAVORized [11] to capture the slow time scale without resolving the fast time scale to greatly reduce integration time. We first give a brief description of FLAVORS (*FLow AVeraging integratORS*). More details can be found in [11]. We also refer to Section 7.6.1 for a mini-discussion on why we chose FLAVORS in this application.

Consider an ordinary differential system on $\mathbb{R}^d$

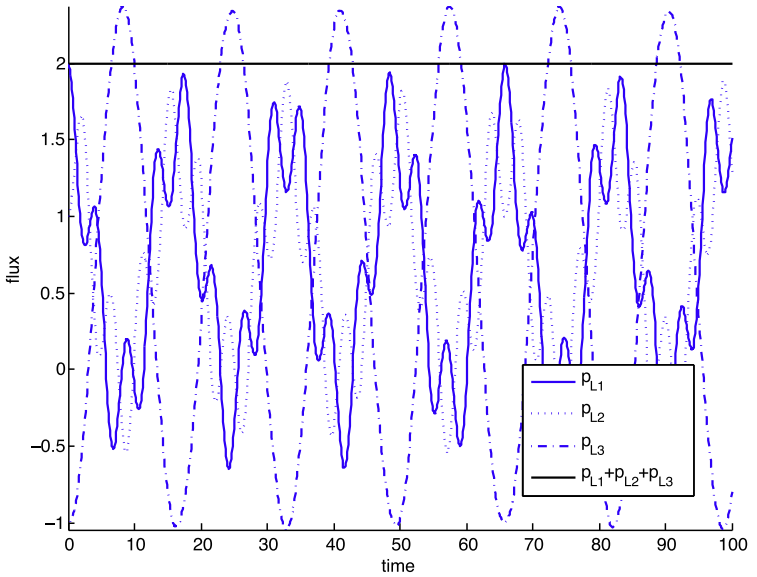


**Fig. 16.** LC transmission line. The sum of the fluxes through all three inductors (blue solid, blue dotted, and blue dashed dotted) is preserved (black line). (For interpretation of reference to colour in this figure legend, the reader is referred to the web version of this article.)

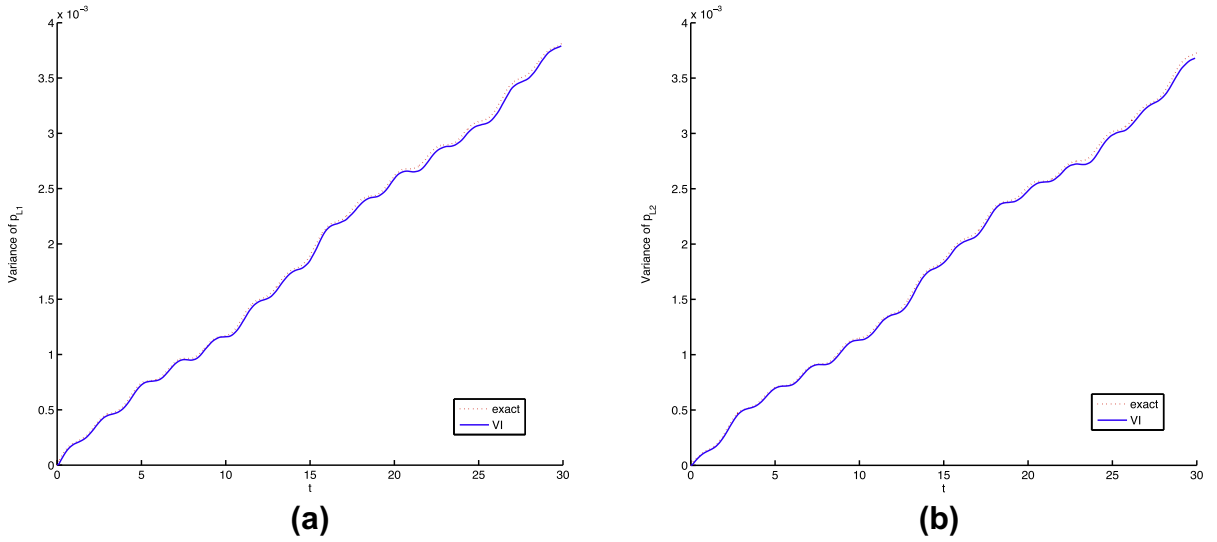


**Fig. 17.** Benchmark of variances as functions of time according to (46b) (red dotted) and variances as functions of time computed numerically by averaging over an ensemble according to (47b) (blue solid). (a) $\mathbb{D}p_1$ (b) $\mathbb{D}p_2$. (For interpretation of the references to colour in this figure legend, the reader is referred to the web version of this article.)

$$\dot{u}^\epsilon = G(u^\epsilon) + \frac{1}{\epsilon}F(u^\epsilon), \tag{48}$$

with $\epsilon \ll 1$. In the context of Lagrangian systems, we consider a multiscale Lagrangian as

$$\mathcal{L}(q, v) = \frac{1}{2}v^T L v - V(q) - \frac{1}{\epsilon}U(q) \tag{49}$$

where $V(q)$ is denoted as "slow" and $\frac{1}{\epsilon}U(q)$ denoted as "fast" potential. In the case of a linear circuit, the slow potential corresponds to the charge potential of a capacitor with high capacitance, whereas the fast potential corresponds to a capacitor with very small capacitance. For instance, consider the oscillating LC circuit in Section 7.3 with $C_1 = 1$ and $C_2 = \epsilon$ ($\epsilon = 1$ in Section 7.3). The corresponding potential in (49) can be written as the sum of slow and fast potential as

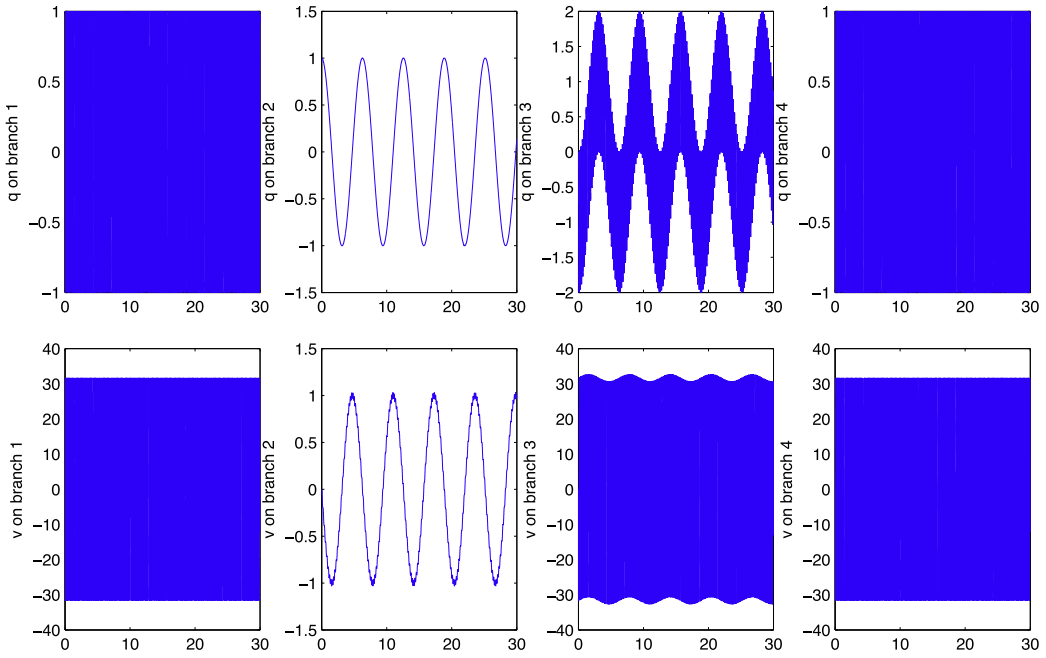


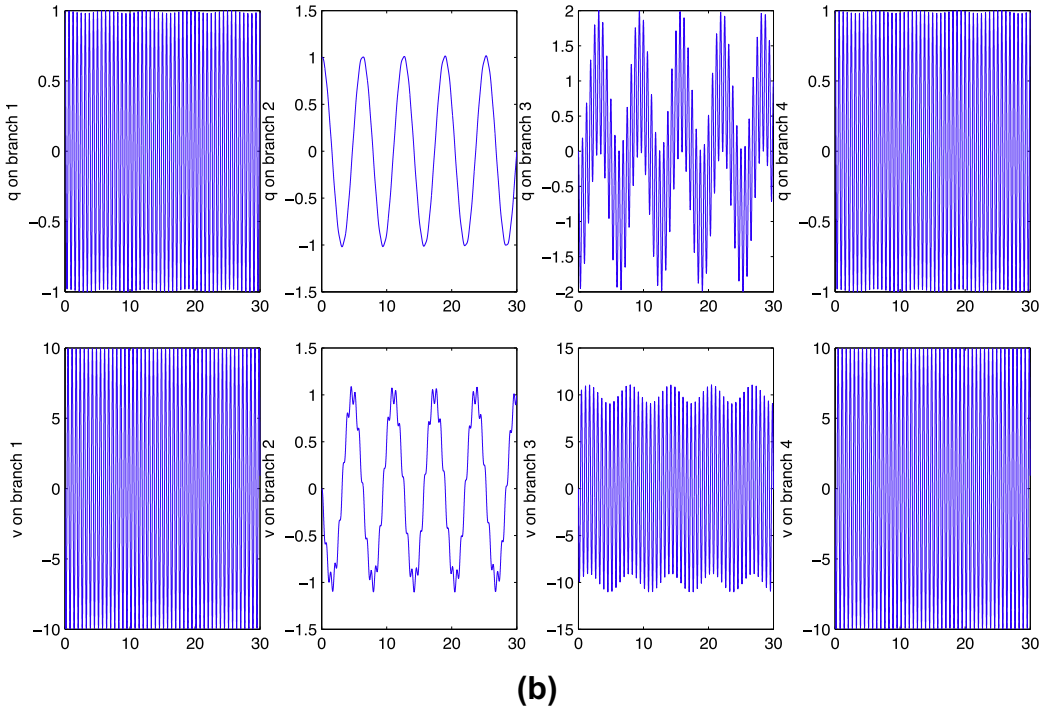


**Fig. 18.** Simulations of a multiscale system: (a) Benchmark solution computed with a variational integrator ($h = 10^{-4}$) (b) FLAVOR with $\tau = 10^{-4}, \delta = 10^{-3}$ and $\epsilon = 10^{-3}$.

$$V(q) = \frac{1}{2} q_{C_1}^2, \quad U(q) = \frac{1}{2} q_{C_2}^2.$$

The smaller $\epsilon$ (i.e., $C_2$) is, the wider the two time scales will be separated.

FLAVORS are based on the averaging of the instantaneous flow of the differential Eq. (48) with hidden slow and fast variables. The way to FLAVORize any of our integrators for circuits is to break each timestep into a composition of two substeps.

The first one uses a timestep of length $\tau$, and the second one uses a timestep $\delta - \tau$. $\tau$ has to be small enough to resolve the stiffness, but $\delta - \tau$ does not. In fact, in the first substep one integrates the entire system with the original value of the stiffness $1/\epsilon$, whereas in the second substep one integrates the system with the stiffness turned off, that is $1/\epsilon$ is temporarily set to 0. Of course, for the first substep of the next step, $1/\epsilon$ has to be restored to its original big value again. To be more precise, FLAVOR is implemented using an arbitrary legacy integrator $\Phi_h^{\frac{1}{\epsilon}}$ for (48) in which the parameter $\frac{1}{\epsilon}$ can be controlled. By switching on and off the stiff parameter, FLAVOR approximates the flow of (48) over a coarse time step $H$ (resolving the slow time scale) by the flow

$$\Phi_H := \left(\Phi^0_{\frac{H}{M}-\tau} \circ \Phi^{\frac{1}{\epsilon}}_{\tau}\right)^M,$$

where $\tau$ is a fine time step resolving the "fast" time scale ($\tau \ll \epsilon$) and $M$ is a positive integer corresponding to the number of "samples" used to average the flow ($\delta = H/M$). Since FLAVORS are obtained by flow composition, they inherit the structure-preserving properties (for instance, symplecticity and symmetries under a group action) of the legacy integrator for Hamiltonian systems.

Theorem 1.4 in [11] guarantees the accuracy of FLAVORS for $\delta \ll h_0, \tau \ll \epsilon$ and $\left(\frac{\tau}{\epsilon}\right)^2 \ll \delta \ll \frac{\tau}{\epsilon}$, where $h_0$ is the stability limit of step length for the legacy integrator. Furthermore, if the hidden fast and slow variables are affine functions of the original variables (such as in our case of linear circuit), the condition relaxes to $\delta \ll h_0, \tau \ll \epsilon$ and $\delta \ll \frac{\tau}{\epsilon}$. An intuitive interpretation of that theorem is, the numerically integrated slow variable will converge strongly (as a function of time) to the solution of an averaged effective equation, and the fast variable will converge weakly to its local ergodic measure.

We use FLAVORS to simulate the LC circuit with $\epsilon = 10^{-3}, \tau = 0.1\epsilon = 10^{-4}, H = 0.1$ and $M = 100$. The charges and currents as functions of time are plotted in Fig. 18. Notice that the slow components in the solution are captured strongly, but the fast components may have altered wave shapes: for instance, Fig. 19 shows a zoomed-in investigation of the current through the second branch, which is a superposition of a slow global oscillation and a fast local oscillation; the slow one is obviously well-captured in the usual sense, and the fast one is captured in the less-commonly-used sense of averaging.

*7.6.1. Mini-discussion on multiscale methods*

Multiscale linear circuits fall in the category of highly oscillatory problems, where after dealing with the circuit constraints (which is nontrivial and one of the main contents of this paper) the problem can be approached by many methods, a non-exhaustive list including integrators based on exponentials (e.g., [42–48]), highly oscillatory quadrature (see for instance [49–53] and references therein), Hamilton–Jacobi approaches [54,55], filtering techniques [56–58], Poincaré map techniques [59,60].

Multiscale nonlinear circuits, however, go beyond the scope of many methods described above. A note on two classes of general multiscale methods, HMM (e.g., [61–64]) and the equation-free method (e.g., [65,66]), is that they may work for nonlinear circuits (again after constraints are handled with); nevertheless, so far there is no symplectic version of these approaches, and hence their applications in simulating circuits are limited, especially at the presence of voltage sources and resistances. Because of this, in this paper, we instead make our circuit integrator multiscale via the approach of FLAVORs [11], which are intrinsically symplectic and in fact variational. Moreover, our framework based on FLAVORs works for nonlinear circuits without any identification of slow or fast variables. Symplecticity in a multiscale simulation, which is a unique

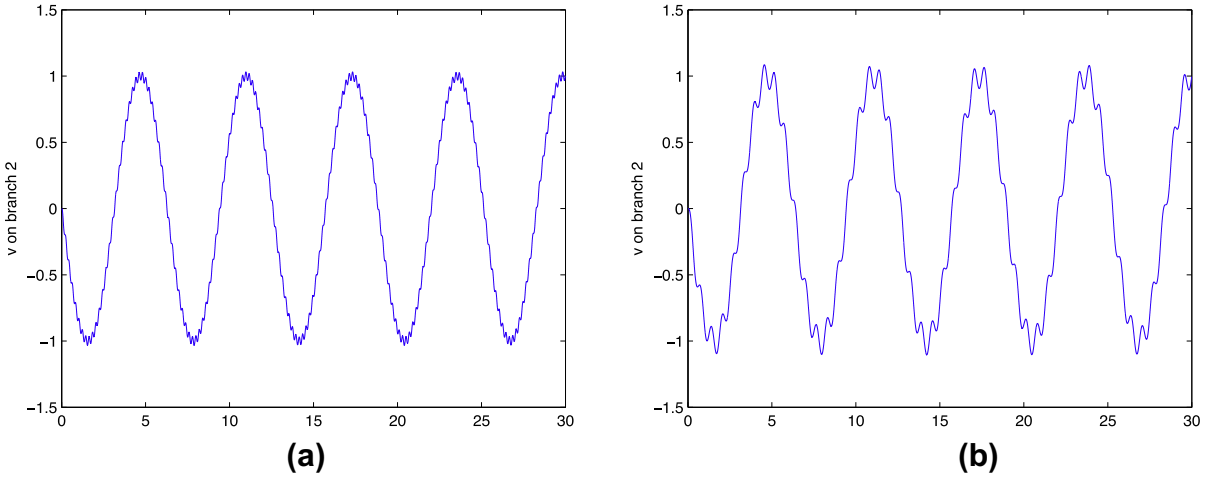


**Fig. 19.** Simulations of a multiscale system: (a) Benchmark solution computed with a variational integrator ($h = 10^{-4}$) (b) FLAVOR with $\tau = 10^{-4}, \delta = 10^{-3}$ and $\epsilon = 10^{-3}$.

feature enabled by FLAVORs, allows us: (1) good long-time performance, (2) correct capture of the effects of voltage sources and resistances, and (3) correct generalization to a stochastic setting.

More precisely, compared to the classical version of HMM [61] the main advantages of FLAVORs are as follows:

- They do not require the detection of slow variables (even with a non-linear relation between original variables and slow variables [67,68]).
- Their implementation is very simple and non-intrusive: an existing/legacy integrator can be FLAVORized, that is it can be turned into multi-scale integrator by adding five lines of code designed to turn on and off the stiff coefficients in that legacy integrator.
- They preserve symmetries and inherit structures preserving properties (such as symplecticty) of the legacy integrator; methods based on drift averaging do not have this property.

We note that a new version of HMM based on a Poincaré map type technique was recently proposed [64]. This new version does not appear to be symplectic, but it does not require the identification of slow variables and it also allows for high order accuracy compared to the basic version of FLAVOR [11]. Constructing higher order multi-scale integrators via flow averaging requires employing higher order splitting methods than the one employed in the basic version of FLAVOR.

## 8. Conclusions

In this contribution, we presented a unified framework for the modeling and simulation of electric circuits. Starting with a geometric setting, we formulate a unified variational formulation for the modeling of electric circuits. Analogous to the formulation of mechanical systems, we define a degenerate Lagrangian on the space of branches that consists of electric and magnetic energy, dissipative and external forces that describe the influence of resistors and voltage sources, as well as (non-) holonomic constraints given by the KCL of the circuit. The Lagrange-d'Alembert-Pontryagin principle is used to derive, in a variational way, the implicit Euler–Lagrange equations. These are differential–algebraic equations and describe the system's dynamics. A reduced version on the space of meshes is presented that is shown to be equivalent to the original system and for which under some topology assumptions the degeneracy of the Lagrangian is canceled.

Based on the reduced version, a discrete variational approach is presented that provides different variational integrators for the simulation of circuits. In particular, the generated integrators are symplectic, preserve momentum maps in presence of symmetries and have good long-time energy bahvior. Furthermore, we observe that the spectrum of high frequencies is especially better preserved compared to simulations using Runge–Kutta or BDF methods. Having the variational framework for the model and the simulation, extensions of the approach by using already-existing types of different variational integrators can be easily accomplished. As an example, we presented the extension for the simulation of noisy circuits by using stochastic variational integrator approaches as well as multiscale methods (in particular FLAVORS) for an efficient treatment of circuits with multiple time scales.

In the future, we will extend the approach to the simulation and analysis of more complicated nonlinear and magnetic circuits that might include nonlinear inductors, capacitors, resistors, and transistors. Since a variational formulation in terms of energies, forces, and constraints is still valid for the nonlinear case, the presented integrators will be derived and applied in straight forward way. Furthermore, the inclusion of controlled sources allows for the consideration of optimal control problems for circuits for which techniques based on a variational formulation can be easily applied (see for example [5]). The variational simulation of combined mechanical and electric (electro-mechanical) systems is the natural next step towards the development of a unified variational modeling and simulation method for mechatronic systems. Furthermore, at nanoscales, thermal noise and electromagnetic interactions become an essential component of the dynamic of electric circuits. We plan to investigate the coupling of variational integrators for circuits with multi-symplectic variational integrators for EM fields and continuum mechanics (see for example [69–71]) to produce a robust structure-preserving numerical integrator for Microelectromechanical and Nanoelectromechanical systems. Recently, Mike Giles has developed a Multilevel Monte Carlo method for differential equations with stochastic forcings [72] that shows huge computation accelerations, 100 times in some cases. The extension of the current method to multilevel stochastic variational integrators is straight forward and may further accelerate the computation dramatically, especially for multiscale problems, while preserving certain properties of the circuit network.

## Acknowledgements

This contribution was partly developed and published in the course of the Collaborative Research Centre 614 "Self-Optimizing Concepts and Structures in Mechanical Engineering" funded by the German Research Foundation (DFG) under Grant No. SFB 614. The authors acknowledge partial support from NSF grant CMMI-092600. The authors gratefully acknowledge Henry Jacobs, Melvin Leok, and Hiroaki Yoshimura for delightful discussions about variational mechanics for degenerate systems. Furthermore, the authors thank Stefan Klus, Sujit Nair, Olivier Verdier, and Hua Wang for helpful discussions regarding circuit theory. Finally, we thank Sydney Garstang and Carmen Sirois for proofreading the document.

## References


[1] J.E. Marsden, M. West, Discrete mechanics and variational integrators, Acta Numerica 10 (2001) 357–514.
[2] A. Lew, J.E. Marsden, M. Ortiz, M. West, An overview of variational integrators, in: L.P. Franca, T.E. Tezduyar, A. Masud (Eds.), Finite Element Methods: 1970's and Beyond, CIMNE, 2004, pp. 98–115.
[3] A. Lew, J.E. Marsden, M. Ortiz, M. West, Variational time integrators, International Journal for Numerical Methods in Engineering 60 (1) (2004) 153–212.
[4] C. Kane, J.E. Marsden, M. Ortiz, M. West, Variational integrators and the Newmark algorithm for conservative and dissipative mechanical systems, International Journal for Numerical Methods in Engineering 49 (10) (2000) 1295–1325.
[5] S. Ober-Blöbaum, O. Junge, J.E. Marsden, Discrete mechanics and optimal control: an analysis, Control, Optimisation and Calculus of Variations 17 (2) (2011) 322–352.
[6] S. Leyendecker, J.E. Marsden, M. Ortiz, Variational integrators for constrained dynamical systems, Journal of Applied Mathematics and Mechanics 88 (9) (2008) 677–708.
[7] S. Leyendecker, S. Ober-Blöbaum, J.E. Marsden, M. Ortiz, Discrete mechanics and optimal control for constrained systems, Optimal Control, Applications and Methods 31 (6) (2010) 505–528.
[8] M. Kobilarov, J.E. Marsden, G.S. Sukhatme, Geometric discretization of nonholonomic systems with symmetries, Discrete and Continuous Dynamical Systems – Series S 1 (1) (2010) 61–84.
[9] R.C. Fetecau, J.E. Marsden, M. Ortiz, M. West, Nonsmooth Lagrangian mechanics and variational collision integrators, SIAM Journal of Applied Dynamical Systems 2 (3) (2003) 381–416.
[10] N. Bou-Rabee, H. Owhadi, Stochastic variational integrators, IMA Journal of Numerical Analysis 29 (2008) 421–443.
[11] M. Tao, H. Owhadi, J.E. Marsden, Nonintrusive and structure preserving multiscale integration of stiff odes, sdes, and Hamiltonian systems with hidden slow dynamics via flow averaging, Multiscale Modeling and Simulation 8 (4) (2010) 1269–1324.
[12] L.O. Chua, J.D. McPherson, Explicit topological formulations of Lagrangian and Hamiltonian equations for nonlinear networks, IEEE Transactions on Circuits and Systems 21 (2) (1974) 277–286.
[13] H.G. Kwatny, F.M. Massimo, L.Y. Bahar, The generalized Lagrange formulation for nonlinear RLC networks, IEEE Transactions on Circuits and Systems 29 (4) (1983) 220–233.
[14] J. Clemente-Gallardo, J.M.A. Scherpen, Relating Lagrangian and Hamiltonian formalisms of LC circuits, IEEE Transactions on Circuits and Systems - I: Fundamental Theory and Applications 50 (10) (2003) 1359–1363.
[15] G.M. Bernstein, M.A. Liebermann, A method for obtaining a canonical Hamiltonian for nonlinear LC circuits, IEEE Transactions on Circuits and Systems 36 (3) (1998) 411–420.
[16] A. Szatkowski, Remark on explicit topological formulation of Lagrangian and Hamiltonian equations for nonlinear networks, IEEE Transactions on Circuits and Systems 26 (5) (1979) 358–360.
[17] H. Yoshimura, J.E. Marsden, Dirac structures and Lagrangian mechanics. Part I: Implicit Lagrangian systems, Journal of Geometry and Physics 57 (2006) 133–156.
[18] H. Yoshimura, J.E. Marsden, Dirac structures and implicit Lagrangian systems in electric networks, in: 17th International Symposium on Mathematical Theory of Networks and Systems, 2006, pp. 1444–1449.
[19] H. Yoshimura, J.E. Marsden, Dirac structures and Lagrangian mechanics. Part II: Variational structures, Journal of Geometry and Physics 57 (2006) 209–250.
[20] L. Moreau, A.J. van der Schaft, Implicit Lagrangian equations and mathematical modeling of physical systems, in: 41st IEEE Conference on Decision and Control, Las Vegas, Nevada, USA, 2002.
[21] H. Jacobs, Y. Yoshimura, J.E. Marsden, Interconnection of Lagrange-Dirac dynamical systems for electric circuits, in: 8th International Conference of Numerical Analysis and Applied Mathematics, vol. 1281, 2010, pp. 566–569. http://dx.doi.org/10.1063/1.3498539.
[22] G. Blankenstein, Implicit Hamiltonian systems: symmetry and interconnection, Ph.D. thesis, University of Twente, 2000.
[23] B.M. Maschke, A.J. van der Schaft, P.C. Breeveld, An intrinsic Hamiltonian formulation of the dynamics of LC-circuits, IEEE Transactions on Circuits and Systems I: Fundamental Theory and Applications 42 (2) (1995) 73–82.
[24] A.M. Bloch, P.R. Crouch, Representations of Dirac structures on vector spaces and nonlinear LC-circuits, in: Differential Geometry and Control (Boulder, CO., 1997), Proceedings of Symposia in Pure Mathematics, vol. 64, American Mathematical Society, Providence, RI, 1997, pp. 103–117.
[25] J. Cervera, A.J. van der Schaft, A. Baños, Interconnection of port-Hamiltonian systems and composition of Dirac structures, Automatica 43 (2007) 212–225, http://dx.doi.org/10.1016/j.automatica.2006.08.014.
[26] C.W. Rowley, J.E. Marsden, Variational integrators for degenerate Lagrangians, with application to point vortices, in: 41st IEEE Conference on Decision and Control, vol. 2, 2002, 1521–1527
[27] M. Leok, T. Ohsawa, Discrete Dirac structures and implicit discrete Lagrangian and Hamiltonian systems, in: GEOMETRY AND PHYSICS: XVIII International Fall Workshop on Geometry and Physics, vol. 1260, AIP Conference Proceedings, 2010, pp. 91–102, http://dx.doi.org/10.1063/1.3479325.
[28] N. Bou-Rabee, H. Owhadi, Long-run accuracy of variational integrators in the stochastic context, SIAM Journal of Numerical Analysis 48 (1) (2010) 278–297.
[29] J.W. Nilsson, S.A. Riedel, Electric Circuits, seventh ed., Prentice Hall, 2005.
[30] J. Gross, J. Yellen, Handbook of Graph Theory, Discrete Mathematics and its Applications, CRC Press, 2004.
[31] N. Bou-Rabee, Hamilton-Pontryagin integrators on Lie groups, Ph.D. thesis, California Institute of Technology, 2007.
[32] P. Kunkel, V. Mehrmann, Differential-Algebraic Equations, EMS Textbooks in Mathematics, European Mathematical Society, 2006.
[33] E. Hairer, C. Lubich, G. Wanner, Geometric numerical integration, Springer Series in Computational Mathematics, vol. 31, Springer, 2002.
[34] N. Bou-Rabee, H. Owhadi, Near Boltzmann-Gibbs measure preserving stochastic variational integrator, Technical Report (December 2007) arXiv:0712.4123, <http://arxiv.org/pdf/0712.4123v1.pdf>.
[35] J.E. Marsden, T. Ratiu, Introduction to Mechanics and Symmetry, Texts in Applied Mathematics, vol. 17, Springer, 1994.
[36] S. Blanes, A. Iserles, Explicit adaptive symplectic integrators for solving Hamiltonian systems, Celestial Mechanics and Dynamical Astronomy (2012) 1–21, http://dx.doi.org/10.1007/s10569-012-9441-z.
[37] S. Voigtmann, General linear methods for integrated circuit design, Ph.D. thesis, Humboldt-Universität zu Berlin, 2006.
[38] M. Günther, U. Feldmann, J. ter Maten, Modelling and discretization of circuit problems, OAI Repository of the Technische Universiteit Eindhoven, Technical report, 2005
[39] S. Bächle, Numerical solution of differential-algebraic systems arising in circuit simulation, Ph.D. thesis, Technische Universität Berlin, 2007.
[40] E. Hairer, G. Wanner, Solving Ordinary Differential Equations II: Stiff and Differential-Algebraic Problems, Springer, 1991.
[41] B. ksendal, Stochastic Differential Equations. An Introduction with Applications, fifth ed., Springer, 2000, ISBN 3-540-63720-6.
[42] H. Grubmuller, H. Heller, A. Windemuth, K. Schulten, Generalized Verlet algorithm for efficient molecular dynamics simulations with long-range interactions, Molecular Simulation 6 (1991) 121–142.
[43] M. Tuckerman, B.J. Berne, G.J. Martyna, Reversible multiple time scale molecular dynamics, Journal of Chemical Physics 97 (1992) 1990–2001.
[44] B. García-Archilla, J.M. Sanz-Serna, R.D. Skeel, Long-time-step methods for oscillatory differential equations, SIAM Journal of Scientific Computing 20 (3) (1999) 930–963.
[45] J.M. Sanz-Serna, Mollified impulse methods for highly oscillatory differential equations, SIAM Journal of Numerical Analysis 46 (2) (2008) 1040–1059.
[46] V. Grimm, M. Hochbruck, Error analysis of exponential integrators for oscillatory second-order differential equations, Journal of Physics A: Mathematical and General 39 (2006) 5495–5507.

[47] M. Hochbruck, C. Lubich, A gautschi-type method for oscillatory second-order differential equations, Numerical Mathematics 83 (1999) 403–426.
[48] M. Tao, H. Owhadi, J.E. Marsden, From efficient symplectic exponentiation of matrices to symplectic integration of high-dimensional Hamiltonian systems with slowly varying quadratic stiff potentials, Applied Mathematics Research Express 2011 (2) (2011) 242–280.
[49] A. Iserles, S. Nrsett, From high oscillation to rapid approximation I: Modified fourier expansions, IMA Journal of Numerical Analysis 28 (2008) 862–887.
[50] B. Adcock, A. Iserles, S. Nrsett, From high oscillation to rapid approximation II: Expansions in birkhoff series, IMA Journal of Numerical Analysis 32 (2012) 105–140.
[51] A. Iserles, S. Nrsett, From high oscillation to rapid approximation III: Multivariate expansions, IMA Journal of Numerical Analysis 29 (2009) 882–916.
[52] D. Huybrechs, A. Iserles, S. Nrsett, From high oscillation to rapid approximation IV: Accelerating convergence, IMA Journal of Numerical Analysis 31 (2011) 442–468.
[53] D. Huybrechs, A. Iserles, S. Nrsett, From high oscillation to rapid approximation V: The equilateral triangle, IMA Journal of Numerical Analysis 31 (2011) 755–785.
[54] C. Le Bris, F. Legoll, Integrators for highly oscillatory hamiltonian systems: an homogenization approach, Discrete and Continuous Dynamical Systems - Series B 13 (2010) 347–373.
[55] M. Dobson, C. Le Bris, F. Legoll, Symplectic schemes for highly oscillatory Hamiltonian systems: the homogenization approach beyond the constant frequency case, IMA Journal of Numerical Analysis, in press.
[56] W. Gautschi, Numerical integration of ordinary differential equations based on trigonometric polynomials, Numerical Mathematics 3 (1961) 381–397.
[57] H.-O. Kreiss, Problems with different time scales, Acta Numerica 1 (1992) 101–139.
[58] R. Scheid, The accurate numerical solution of highly oscillatory ordinary differential equations, Mathematics of Computation 41 (164) (1983) 487–509.
[59] C. Gear, K. Gallivan, Automatic methods for highly oscillatory ordinary differential equations, in: Numerical analysis (Dundee, 1981), Lecture Notes in Mathematics, vol. 912, Springer, Berlin, 1982, pp. 115–124.
[60] L. Petzold, L. Jay, J. Yen, Problems with different time scales, Acta Numerica 6 (1997) 437–483.
[61] W.E.B. Engquist, X. Li, W. Ren, E. Vanden-Eijnden, Heterogeneous multiscale methods: a review, Communications in Computational Physics 2 (3) (2007) 367–450.
[62] W. E, Analysis of the heterogeneous multiscale method for ordinary differential equations, Communications in Mathematical Sciences 1 (3) (2003) 423–436.
[63] G. Ariel, B. Engquist, Y.-H. Tsai, A multiscale method for highly oscillatory ordinary differential equations with resonance, Mathematics of Computation 78 (2009) 929.
[64] G. Ariel, B. Engquist, S. Kim, Y. Lee, R. Tsai, A multiscale method for highly oscillatory dynamical systems using a poincaré map type technique, Journal of Scientific Computing (2012) 1–22, http://dx.doi.org/10.1007/s10915-012-9656-x. http://dx.doi.org/10.1007/s10915-012-9656-x .
[65] I.G. Kevrekidis, C.W. Gear, J.M. Hyman, P.G. Kevrekidis, O. Runborg, C. Theodoropoulos, Equation-free, coarse-grained multiscale computation: enabling microscopic simulators to perform system-level analysis, Communications in Mathematical Sciences 1 (4) (2003) 715–762.
[66] I. Kevrekidis, G. Samaey, Equation-free multiscale computation: Algorithms and applications, Annual Review of Physical Chemistry 60(1), 2009, pp. 321–344. http://dx.doi.org/10.1146/annurev.physchem.59.032607.093610, <http://arjournals.annualreviews.org/doi/abs/10.1146/annurev.physchem.59.032607.093610> (pMID: 19335220, arXiv:http://arjournals.annualreviews.org/doi/pdf/10.1146/annurev.physchem.59.032607.093610).
[67] W. E, D. Liu, E. Vanden-Eijnden, Nested stochastic simulation algorithms for chemical kinetic systems with multiple time scales, Journal of Computational Physics 221 (1) (2007) 158–180, http://dx.doi.org/10.1016/j.jcp. 2006.06.019. http://dx.doi.org/10.1016/j.jcp.2006.06.019 .
[68] E. Vanden-Eijnden, On HMM-like integrators and projective integration methods for systems with multiple time scales, Communications in Mathematical Sciences 5 (2) (2007) 495–505. <http://projecteuclid.org/getRecord?id=euclid.cms/1183990377> .
[69] A. Lew, Variational time integrators in computational solid mechanics, Ph.D. thesis, California Institute of Technology, 2003.
[70] J.E. Marsden, S. Pekarsky, S. Shkoller, M. West, Variational methods, multisymplectic geometry and continuum mechanics, Journal of Geometry and Physics 38 (3–4) (2001) 253–284.
[71] A. Stern, Y. Tong, M. Desbrun, J.E. Marsden, Geometric computational electrodynamics with variational integrators and discrete differential forms, preprint, 2009. arXiv:0707.4470.
[72] M.B. Giles, Multilevel Monte Carlo path simulation, Operations Research 56 (3) (2008) 607–617.